Alma Mater Studiorum - Università di Bologna

SCUOLA DI SCIENZE

Dipartimento di Chimica Industriale “Toso Montanari”

Corso di Laurea Magistrale in

Chimica Industriale

Classe LM-71 - Scienze e Tecnologie della Chimica Industriale

Fracture toughness characterization of aluminium-epoxy adhesive joints reinforced with electrospun Nylon 6,6 nanofibers

Tesi di laurea sperimentale

CANDIDATO

Enrico Leoni

RELATORE

Chiar.ma Prof.ssa Laura Mazzocchetti

CORRELATORI

Davide Cocchi

Emanuele Maccaferri

Anno Accademico 2018-2019

SUMMARY

1. STATE OF ART AND BACKGROUND

An adhesive may be defined as a non-metallic (polymeric) material which is able to join two different substrates (made of the same or also different materials) and to resist separation using both adhesion mechanisms (developed between the adhesive and the substrate) and cohesive mechanisms (developed within the adhesive itself).

The adhesive is usually in a liquid state when applied and reach a solid state after curing and relatively small quantities are required compared to the weight of the final components [1].

In Section 1.1, a brief introduction about adhesives is presented and mechanisms of adhesion are shown in Section 1.2. In Section 1.3, epoxy adhesives are described in deep given that they are the class that will be used in the present work and one of the most commonly used in general. Nowadays, different methods to increase fracture toughness are available: the most important are discussed in Section 1.4. In particular in Section 1.5 and 1.6, the production process of nanofibers, adopted in this work as adhesive reinforcement, is shown. In order to obtain a substrate suitable for bonding, surface treatments are necessary; the most significative are explained in Section 1.7 . Finally, at the end of the production process, fracture toughness of the joint is quantified by means of Double Cantilever Beam (DCB) test in Section 1.8.

1.1 Advantages and limitations of adhesives

The use of adhesive methods to join materials in substitution of classic technologies such as welding, soldering, riveting or brazing is becoming more and more used in the recent years, in particular for automotive and aerospace industries.

According to [2], advantages of adhesives over other joining techniques are listed below:

- the ability to join the majority of materials, even to make joints between different materials;
- an improved stress distribution in the joint, reducing the stress concentrations caused by rivets or bolts;
- the potential weight reduction of the structure, mainly because of the ability to join thin-sheet materials efficiently and because adhesives are mostly made of lightweight polymers (whereas screw or bolts are made of metals);

- the capacity to seal, insulate (heat and electricity) and damp vibrations; these properties are a consequence of the composition of the adhesive;
- less expensive than other types of joints, especially when bonding large areas and/or when rapid, low-cost and automated production processes are needed.

On the other hand, some drawbacks are also present:

- surface preparation is one of the most crucial steps of the entire adhesion process, in particular if adhesive joints operate in hostile environments;
- use under extremely high temperature is not recommended;
- disassembly cannot be carried out without incurring in significant damage; recycling is also complex for the same reason;
- there is a limited number of non-destructive test methods for adhesive joints compared to the quantity of those used with other fastening methods;
- heat and pressure are commonly required for a good assembly;
- jigs and fixtures are normally necessary for joining;
- the maximum strength of adhesive joints is relatively low compared to mechanical joints.

1.2 Mechanisms of adhesion

Talking about mechanisms of adhesion, there is no universal theory that can explain in a complete way all interactions that take place inside the joints [1].

There are different theories, each of them applicable only in certain circumstances and often a combination of two or more mechanisms takes place at the same time; these theories allow us to make predictions, to obtain a qualitative evaluation of joint strength and to understand how adhesion works.

Adhesive forces hold two different materials together at their surface, while cohesive forces hold adjacent molecules of a single material together. Both are the result of different forces existing at atomic and molecular level; van der Waals forces (most important forces relative to adhesion), hydrogen bonding and ionic, covalent, or coordination bonds.

Metallic bonds are all short-range forces and commonly result from welding or soldiering, while covalent bonds are the consequence of chemical reactions.

In the following sections, all the different mechanisms of adhesion will be described singularly starting from adsorption theory (Paragraph 1.2.1), mechanical theory (Paragraph 1.2.2), electrostatic theory (Paragraph 1.2.3), diffusion theory (Paragraph 1.2.4) and weak-boundary layer theory (Paragraph 1.2.5).

1.2.1 Adsorption theory

The adsorption theory states that adhesion results from molecular contact between two materials and the surface forces that develop [3].

Adhesive molecules are absorbed onto the surface of the substrate, generating attractive forces designated as secondary or van der Waals forces; given that these are short-range forces, the two surfaces must not be divided by more than a 5 Å distance. The process of establishing a continuous contact between the adhesive and the surface that needs to be bonded is called *wetting*.

As reported in Figure 1, good wetting is obtained when the adhesive spreads over the solid surface (Figure 1a), flowing into the valleys of the substrate surface, while poor wetting takes place when the adhesive leaves those little pores empty (Figure 1b), reducing the area of contact between the adhesive and the adherends [2].

Figure 1 - Examples of (a) good and (b) poor wetting [3].

Wetting can be determined by contact angle measurements, governed by the Young equation, which relates the equilibrium contact angle, θ, generated by the wetting component on the substrate to the appropriate interfacial tensions. A general contact angle example scheme is reported in Figure 2.

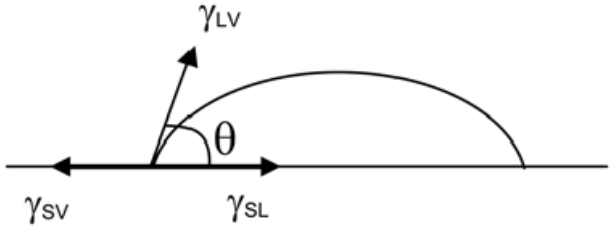

Figure 2 – Contact angle scheme [2].

The Young theory is governed by the following equation:

$$\gamma_{LV} \cdot \cos\theta = \gamma_{SV} - \gamma_{SL}$$

Where γ_{LV} is the surface tension of the fluid material in equilibrium with its vapor, γ_{SV} is the interfacial tension of the solid material in equilibrium with a fluid vapor and γ_{SL} is the interfacial tension between the solid and liquid materials. Obviously, if the wetting is complete and spontaneous, the contact angle is $\theta = 0°$; again, complete or spontaneous wetting occurs when:

$$\gamma_{SV} > \gamma_{LV} + \gamma_{SL}$$

in other words, it happens when the substrate surface tension, γ_{SV}, or its critical surface energy, $\gamma_{C,}$ is high, and the surface tension of the wetting liquid, γ_{LV}, is low. But low energy polymers easily wet high energy substrates such as metals; this explains why epoxies offer excellent adhesion to metals but poor adhesion to polymeric substrates such as PTFE, PE or PP. In conclusion good wetting with epoxies takes place when:

$$\gamma_{adhesive} adhesive << \gamma_C\ substrate$$

To conclude, once continuous contact is achieved between adhesive and adherends, adhesion and cohesion are believed to occur through four types of chemical bonds: electrostatic, metallic and covalent (primary bonds) and van der Waals forces (secondary bonds).

1.2.2 Mechanical theory

The surface of a material is never truly smooth but consists of a series of peaks and cavities; according to the mechanical theory, the adhesive, in order to fully exploit its function, must penetrate these irregularities, displace the trapped air at the interface and lock-on mechanically to the substrate [3].

So, roughness is necessary to improve adhesion; grit blasting, sand blasting and chemical etching are only few methods to achieve that purpose. Interestingly, chemical etching not only modifies the roughness of the surface, but also improves chemical modification of the substrate.

The improvement in roughness gives “teeth” to the substrate and it increases the specific contact area between the adhesive and the adherends, and so the contact surface. In addition, the total surface energy, which is the basis for adhesion, is enhanced.

Another benefit of mechanical interlocking is that a rough surface will provide a crack propagation barrier.

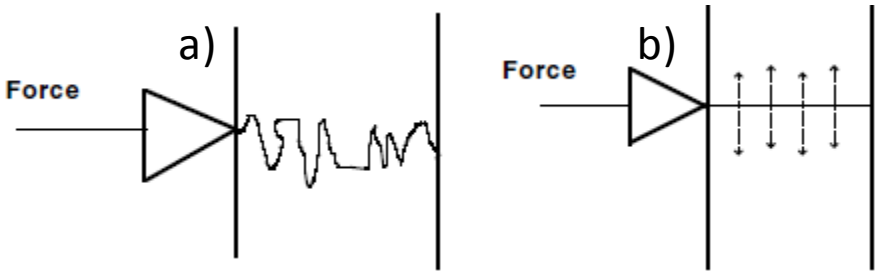

Figure 3 – (a) Rough interface site and (b) smooth interface site [3].

In Figure 3 two different surface topologies are represented. In Figure 3a is clear that the tortuous surface between the adhering materials will act as an obstacle to the crack propagation; the crack goes forward, but the cavities make it to dissipate energy, resulting in an increase of the strength of the joint. In addition to this, the roughness causes the adhesive to plastically deform and thus to adsorb energy. Instead, in the second configuration (Figure 3b), the application of a small force is required to separate the adherends and therefore small energy dissipation occurs; the substrates will simply "unzip".

In the end, mechanical anchoring of the adhesive appears to be a prime factor in bonding many porous substrates; so, fundamental characteristics for good adhesion are: mechanical interlocking, formation of a clean surface, formation of a highly reactive surface, formation of a larger surface.

Unfortunately, this theory is not able to explain some cases when good adhesion occurs between smooth surfaces: mechanical effects are not always of prime importance.

1.2.3 Electrostatic theory

This theory proposes that adhesion takes place due to the formation of an electrical double layer at the adhesive-adherend interface [3]; this double layer is generated by the equilibration of the Fermi levels of both metal (adherend) and polymer (adhesive), assisted by the different nature of the materials which facilitates the transfer of electrons from the metal to the adhesive.

The theory gathers support from the fact that electrical discharges and light flashes have been noticed when an adhesive is peeled off from the substrate.

It is not clear if such electrostatic forces promote an increase of the joint strength or they are a result of that increase [4] but this mechanism is widely accepted as theory for biological cell adhesion.

1.2.4 Diffusion theory

This theory suggests that adhesion is developed through the inter-diffusion of molecules in the adhesive and adherends; the diffuse interfacial layer has generally a thickness between 1-100 nm [1][3] First, the theory is applicable when adhesive and substrate are both polymers, having compatible long-chain molecules capable of movement (they have to be compatible and miscible).

This theory demonstrates the autohesion (spontaneous bonding between two unvulcanised surfaces of an elastomer) of plastics using hot or solvent welding [2]. No stress concentration is present at the interface because no discontinuity exists in the physical properties.

Unfortunately, the diffusion theory can be applied only to a limited number of thermoplastics.

1.2.5 Weak-boundary-layer theory

This theory does not describe an actual adhesion mechanism but instead it allows to explain the lack of adhesion in many cases [2].

In particular it explains that when bond failure seems to be at the interface, usually a cohesive fracture of a weak boundary layer (oxide, oil, low molecular weight species) is the real event [5], and this suggests that a true interfacial failure seldom occurs.

Weak boundary layers can occur on the adhesive or on the adherend, originating from them, from the environment or a combination of the three.

The life of an adhesive joint can be divided into three periods of time:

1. Before application of the adhesive: the surface must be cleaned in order to remove weak boundary layers. The most common examples are atmospheric air and weak oxides such as iron and copper oxides (aluminium oxide is much stronger and does not impair joint strength).
2. Adhesive setting: solidification occurs. If a new weak boundary layer forms during this stage, the joint will be weak. An example can be a chemical reaction by-product of the setting reaction.

3. Service period: in this stage weak boundary layers could occur by environmental moisture diffusing through either the adhesive or the adherends and setting at their interface. In addition to that, low molecular weight species such as plasticizers and solvents may migrate out of the adhesive and deposit at the interface with time.

1.3 Epoxy adhesives

One particular type of adhesives are epoxy adhesives. They are synthesized through the reaction that occurs between epichlorohydrin and bisphenol-A, showed in Figure 4; the product of this reaction is Bisphenol A diglycidyl ether (DGEBA or BADGE), which is the epoxy resin monomer.

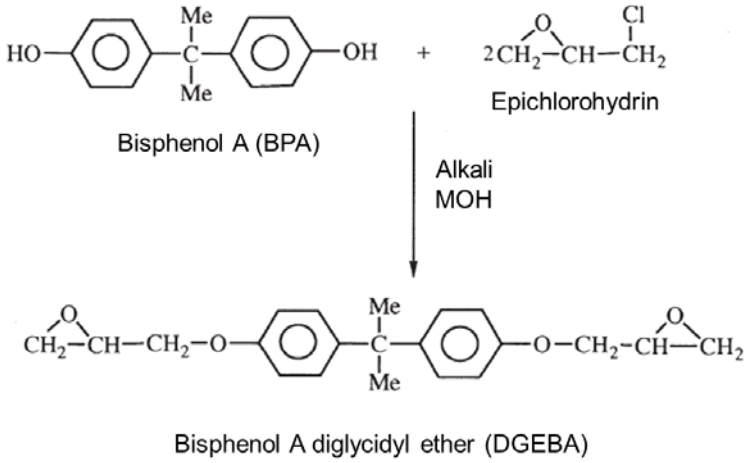

Figure 4 – DGEBA formation reaction [6].

The DGEBA monomer reacts with other molecules of Bisphenol-A and the products of this reaction is a DGEBA oligomer, reported in Figure 5.

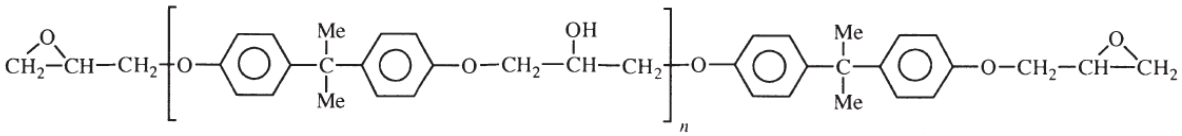

Figure 5 – DGEBA oligomer [6].

Cross-linking of this oligomer occurs with the use, among the other, of tetrafunctional aliphatic or aromatic amines. Aliphatic amines are the most used; aromatic ones can be used too but they are less reactive (and much more toxic) thus they need higher

temperature to start cross-linking and they confer to the resin higher stiffness and then fragility.

Aliphatic amines act following the steps reported below:

1) Diamine attacks the epoxy carbon, as reported in Figure 6.

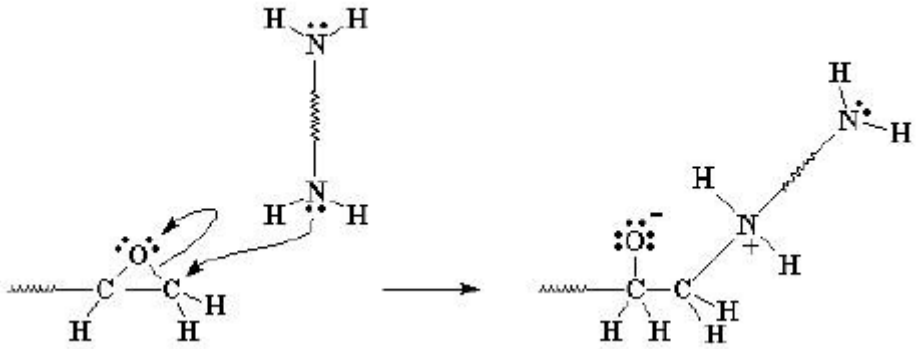

Figure 6 – Attack of the amine to the epoxy carbon atom.

2) An electronic rearrangement occurs: an alcoholic and an amino group are formed as showed in Figure 7.

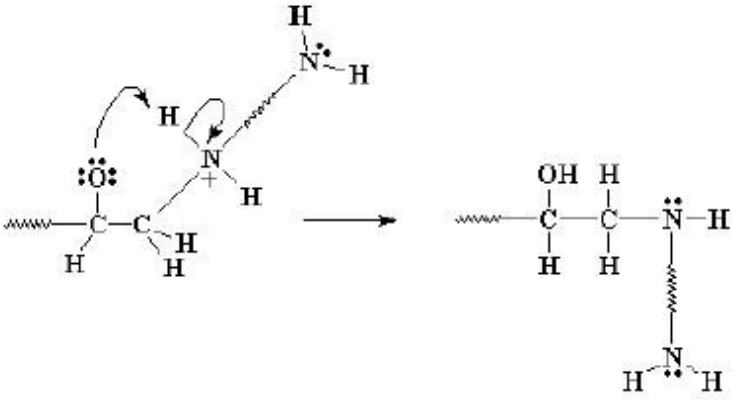

Figure 7 – Electronic rearrangement to form an alcoholic and an amino group.

3) The aminic group can react with as many epoxy group as the number of hydrogen atoms on the amine, as reported in Figure 8.

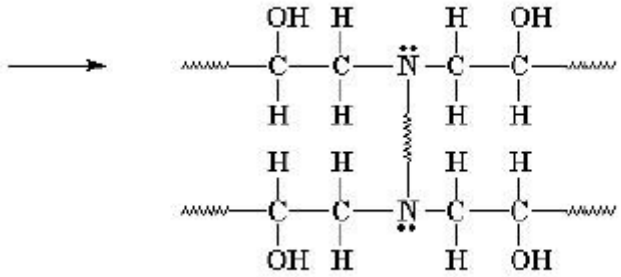

Figure 8 – Formation of the crosslinked structure typical pf epoxy resins.

In this way, every diamine and epoxy molecules reacts and generates a three dimensional crosslinked structure: the epoxy resin.

1.4 Methods to increase the toughness of the joints

There are two leading methods that are useful to increase fracture toughness of adhesive joints:

- addition of nanofillers, which will be described in the paragraphs below and which is the central theme of the present work;
- chemical modification of the resin, which won't be analysed in the present work.

As reported in the chapter above, two main aspects take part in the process of adhesion: mechanical (for example for what concerns mechanical interlocking) and chemical (for examples diffusion as well as adsorption theory).
In this chapter instead, the focus will be moved on a third aspect: nano-reinforcement. Its introduction leads to the fulfilment of the hierarchical scale of the material, as showed in Figure 9.

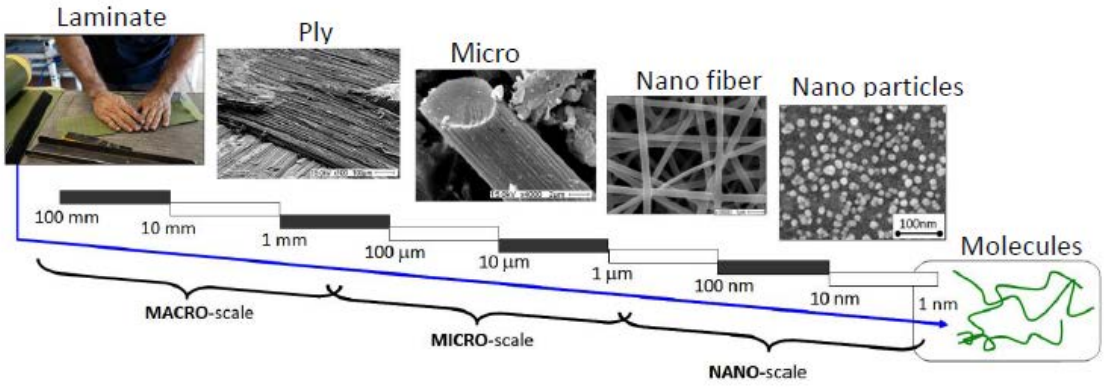

Figure 9 - Hierarchical structure of composite laminates completed by micro and nanofibers [7].

Nano-reinforcements are of fundamental help because with their high surface area, they pledge a substantial contact area between them and the adhesive.
This is the main reason why a lot of research is centred on the use of nano-structured reinforcements (e.g. nanoparticles, nanoplatelets, nanofibers and carbon nanotubes) in order to enhance the strength and toughness of adhesive.

1.4.1 Addition of nanoparticles

Nanoparticles are particles with diameters below 100 nanometres (nm) with a surrounding interfacial layer. They are of great scientific interest because they are a bridge between bulk and molecular structures. A SEM image that shows the aspect of TiO_2 nanoparticles is reported in Figure 10.

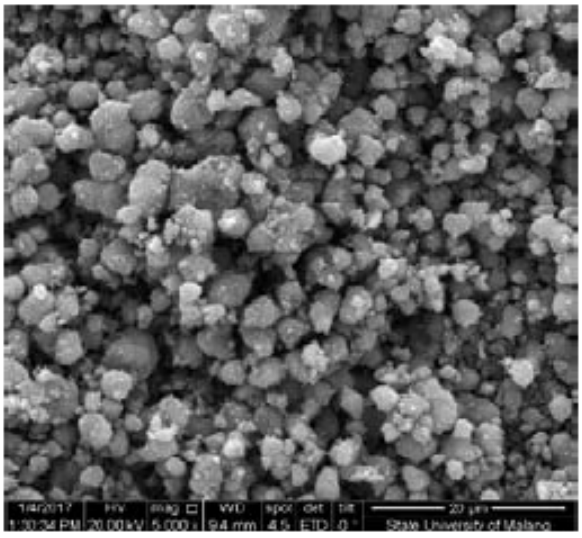

Figure 10 – SEM image of TiO_2 nanoparticles [8].

Due to their nano dimensions (higher surface area and surface/volume ratio), nanoparticles can affect neat polymers properties under different aspects: heat and electricity conduction, thermal stability, mechanical properties and fracture toughness. For example, Dorigato et al. [9] analyse the role of alumina nanoparticles (untreated and calcinated fuming alumina) as a reinforcement of epoxy adhesives. The introduction of untreated alumina nanoparticles brings an improvement of 25% as compared to the pure epoxy resin, up to a filler content of 1.5 vol.%. For concentrations higher than the value reported before, a small reduction of the elastic modulus occurs, probably because of the nanofiller aggregation. For what concerns fracture toughness, the addition of untreated alumina nanoparticles leads to remarkable improvements of

the G_{IC} value (84% higher than the unfilled adhesive) and a slight enhancement of K_{IC} value (13% with respect to the neat matrix).

An alternative to inorganic nanoparticles is the use of elastomeric nanoparticles, as reported by Q. Meng et al. in [10]. Epoxy resin is cured with liquid rubber, a butadiene - acrylonitrile copolymer terminated by amine groups; the use of this type of nanoparticles has been found to produce an improvement of about 50 times in adhesive toughness and a 95% improvement in adhesive bond shear strength. Such an enhancement is possible because nanoparticles have an extremely high interface region with matrix and thus, they can produce a large surface of matrix deformation to absorb fracture energy, which would reduce the chance of interface debonding. An example of rubber nanoparticles dispersion is reported in Figure 11.

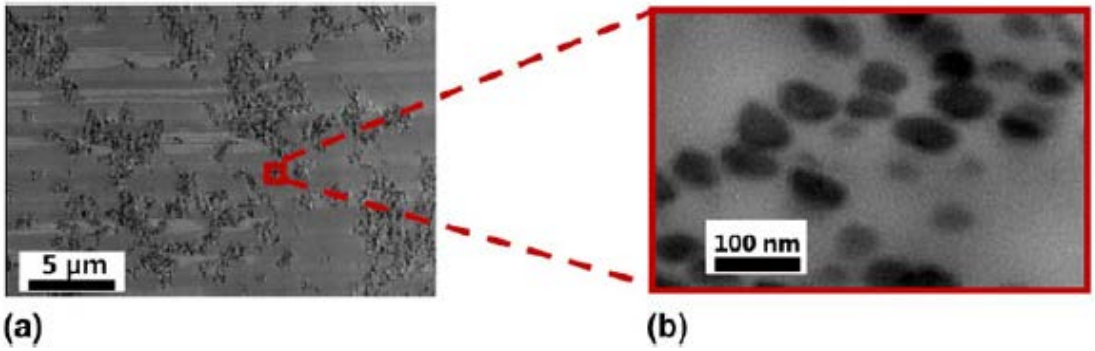

Figure 11 - TEM micrographs of cured epoxy/rubber nanocomposite at 5 vol%: (a) dispersion overview and (b) a magnified cluster [7].

The ductility of nanoparticles plays a fundamental role in producing a marked toughness improvement as well: for example, silica nanoparticles are stiff and do not proceed with cavitation to induce a large-scale matrix deformation; they generate only a thin plastic deformation zone along the crack propagation direction.

1.4.2 Addition of nanoplatelets

Nanoplatelets are a particular type of nanoparticles with only the thickness dimension in the order of nano-meter, whereas their diameter ranges from sub micro-meter to 100 micro-meters; graphene oxide nanoplatelets (GOPs) are the most used. They are made of a certain number of graphene sheets stacked one on another, as exemplified in Figure 12.

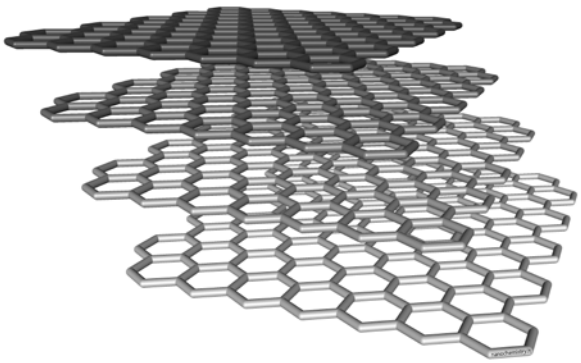

Figure 12 – Nanoplatelets morphology [12].

Khoramishad et al. [13], studied the adhesive fracture behaviour of an epoxy-based adhesive after dispersion of GOPs inside it.

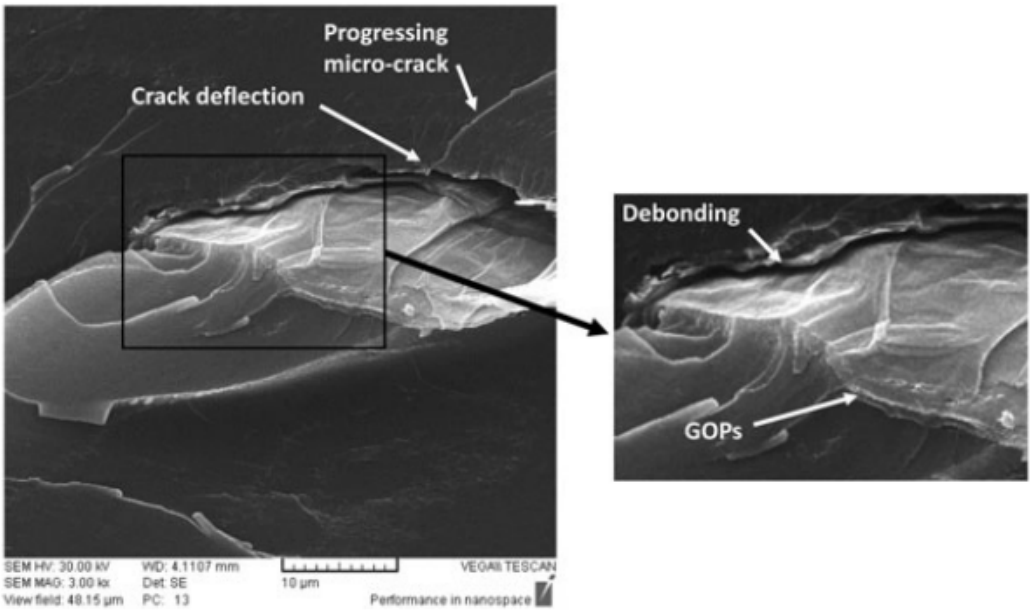

Figure 13 - SEM micrograph of GOP debonding and crack deflection effect [13].

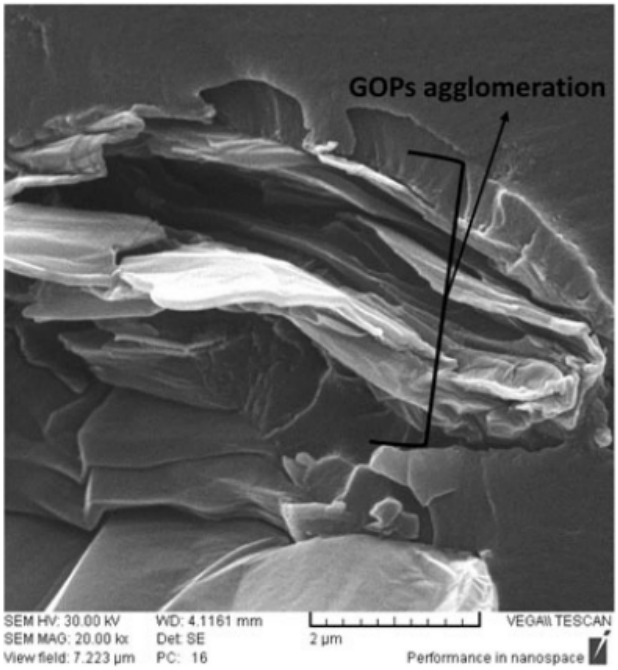

Figure 14 – GOPs agglomeration [13].

The addition of 0.3 wt% of GOPs resulted in an improvement of 69% in the fracture energy of adhesive, while the addition of 0.5% of GPOs caused the decreasing of the adhesive fracture energy. In Figure 13, SEM micrographs suggested GOPs debonding and crack deflection as toughening mechanism; in Figure 14 instead, SEM micrographs demonstrated the agglomeration of the nanofiller, which was no more homogeneously distributed.

1.4.3 Addition of carbon nanotubes

Another form of nanostructure based on carbon are carbon nanotubes (CNTs); they are made of one (single walled carbon nanotubes, SWCNTs) or more (multi walled carbon nanotubes, MWCNTs) graphene sheets bent and joined in one direction so as to form a hollow cylinder. In Figure 15 a scheme of a MWCNT is reported.

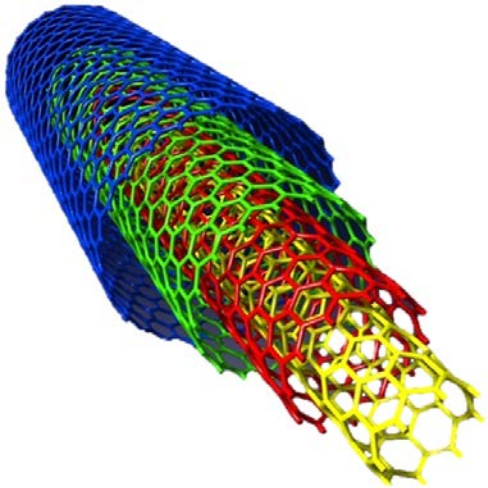

Figure 15 – MWCNT morphology [14].

An example of CNTs reinforced adhesive is reported in [15], where the effect of addition of aligned and randomly dispersed MWCNTs was investigated on the mechanical and fracture behaviours of adhesive joints under mode-I loading. MWCNTs were added to the adhesive layer in either forms of randomly dispersed or aligned (via DC electric field) in the adhesive thickness direction. The addition of randomly dispersed MWCNTs in the percentage of 0.3 wt% lead to a maximum improvement of 55% in the strength of adhesive joints, while the addition of aligned MWCNTs at the same concentration reported above causes a maximum improvement of 88%.

For what concerns the effects relative to the mode-I fracture energy, randomly dispersed and aligned MWCNTs cause an improvement of 135% and 160%, respectively.

A comparison of the effect of random and aligned MWCNT, added at different weight percentage, is reported in the Figure 16 below.

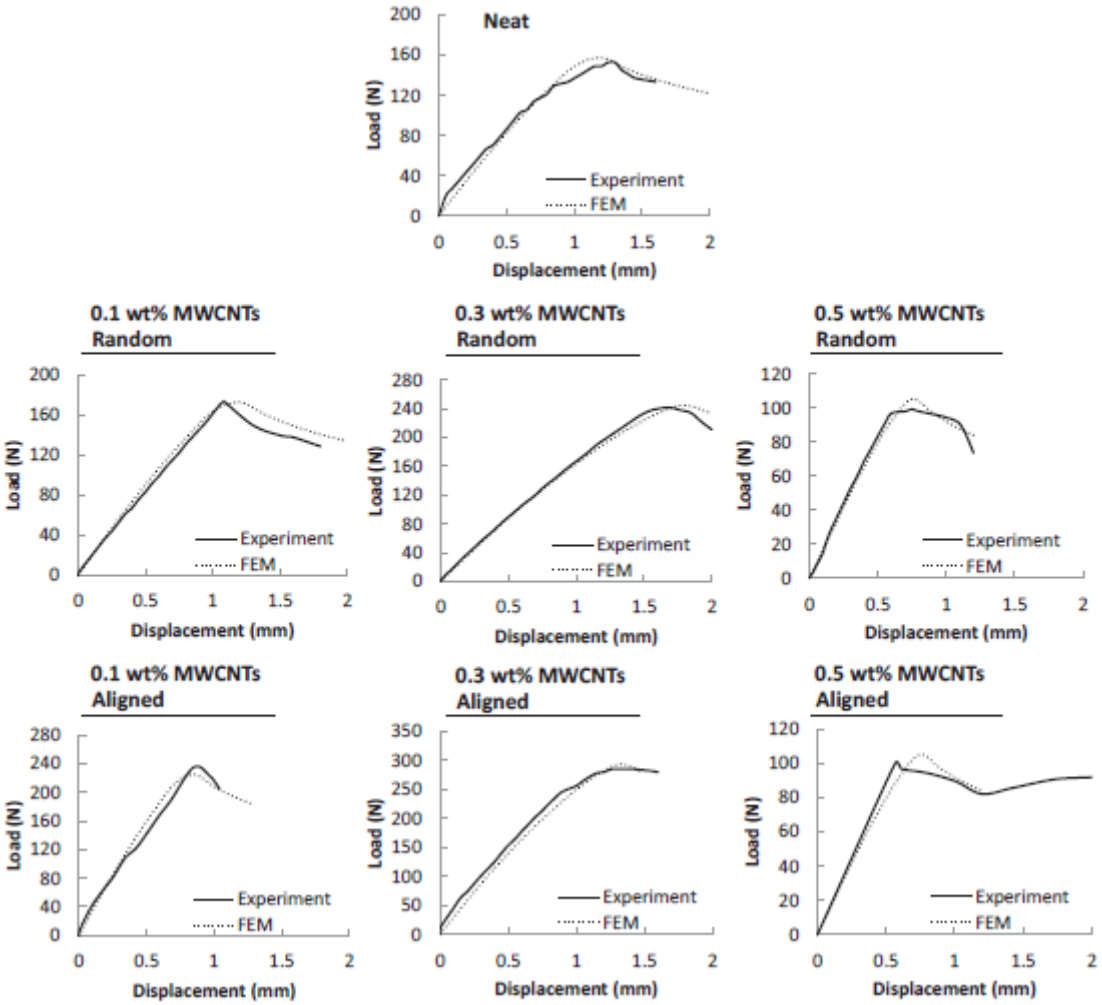

Figure 16 - Comparison between the experimental and numerical load-displacement curves [15].

1.4.4 Addition of nanofibers

Nanofibers are fibres with diameters in the nanometre range (< 1000 nm). One of the most common methods employed to produce nanofibers is the electrospinning process, which will be described accurately in Section 1.6.

An example of nanofibrous mat morphology is reported in Figure 17 where an extremely high porosity can be observed.

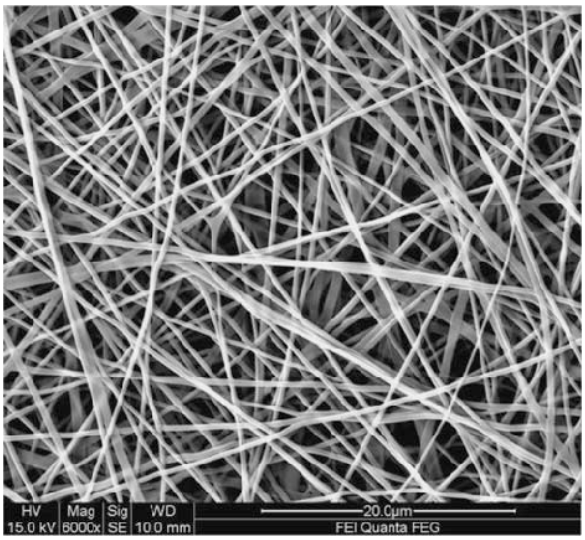

Figure 17 – Morphology of electrospun nanofibrous mat [16].

The use electrospun nanofibers guarantees the satisfaction of the following factors that govern fibres contribution in the composite material [17][18].

1. Basic mechanical properties of the fibres: electrospun nanofibers are virtually continuous nanofibers and have high aspect ratio (L/d); the high elongation of the solidified jet leads to the alignment of the polymer molecular chains, producing mechanically strong fibres. In addition to this, they do not present edges that could act as stress concentration zones.
2. Interface between fibres and polymer matrix: thank to their small diameter, nanofibers exhibit a high specific surface area; this feature leads to an improvement of interfacial bonding strength between reinforcement and matrix higher than that of conventional fibres.
3. Homogeneous fibre dispersion and orientation: the use of the electrospinning process allows to produce mats of unidirectional nanofibers as well as random orientated ones.

Nanofibers are used as a reinforcing method in a wide range of fields, thanks to the characteristics listed above. Nowadays different nanofibre materials are available in literature, as reported in [19]; here the most commonly used are reported and discussed.

The first type of nanofibers presented are carbon nanofibers (CNFs). There are a lot of papers that analyse the use CNFs instead of classical carbon fibres as nanofillers to boost mechanical properties; this happens because it has been widely and well

demonstrated that the mechanical strength of carbon fibre increases with decrease of its diameter [18]. Obviously, electrospinning process is really helpful to achieve this target.

Similar to conventional carbon fibre production, the use of poly-acrylonitrile (PAN) as precursor polymer for electrospun carbon nanofibers (ECNFs) is common; the problem with the use of nanofibers obtained from electrospun PAN is the difficulty in obtaining the required mechanical strength for them to be used as reinforcing fillers, while it is common to see them used for energy storage and conversion, catalysis, sensor and biomedical applications based on their high specific surface area [18].

One of the few examples that demonstrates the potential of ECNFs as reinforcing agent in polymer nano-composite is reported in [20]. In this work, for the first time, ECNFs (with diameters of 200nm and lengths of 15μm) were investigated for the preparation of nano-epoxy resins and, after that, for the fabrication of hybrid multi-scale composites with conventional carbon fibres. After being cut at the above-mentioned length, ECNFs were surface-functionalized with hexanediamine (HDA) so interfacial adhesion between nanofibers and epoxy matrix could be improved (HDA and more in general amines are often used as hardeners for epoxy resins). For comparison, vapor growth carbon nanofibers (VGCNFs) and graphite carbon nanofibers (GCNFs) were also studied for the same purpose; it is noteworthy that while VGCNFs and GCNFs are prepared with the bottom-up methods, ECNFs are produced with the top-down approach. In addition to this, it is useful to say that ECNFs are the most cost-effective between the three types of carbon nanofibers.

The study concluded that the incorporation of 0.5 wt.% of ECNFs-HDA into epoxy resins leads to an enhancement on impact absorption energy (17.3%), tensile strength (22.5%) and flexural properties all together (for example, elastic modulus improved by 14.6%) compared to neat resin. The enhancement of the listed properties is more significant for what concerns ECNFs than VGCNFs and GCNFs.

The prepared nano-epoxy resins were further studied to fabricate multi-scale CFRP composites via vacuum-assisted resin transfer moulding (VARTM) technique; the three types of CNFs led to similar enhancements of mechanical properties of the resulting hybrid multi-scale composites (ECNFs and VGCNFs outperformed GCNFs slightly). Figure 18 represents different morphologies of the three types of surface-functionalized CNFs analysed in this paper.

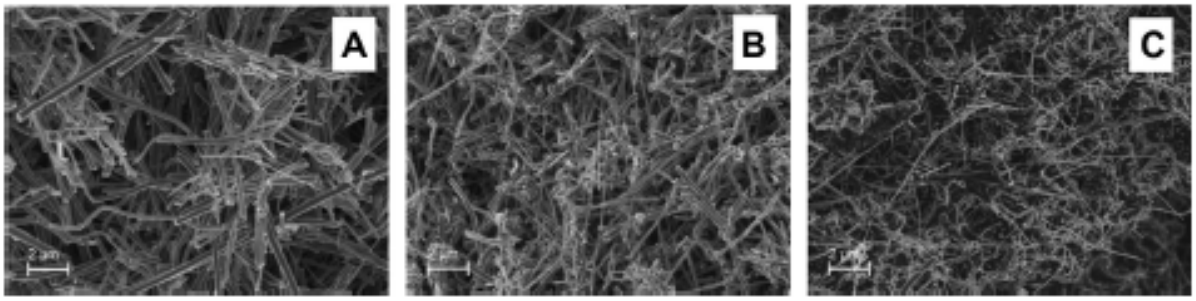

Figure 18 - SEM images showing the representative morphologies of HDA surface-functionalized CNFs: (A) ECNFs-HDA, (B) VGCNFs-HDA, and (C) GCNFs-HDA [20].

To cite another example were carbon nanofibers are used for different purposes other than reinforcement, in [21] is described the fabrication of a functionalized ECNF containing calcium phosphate nanoparticles (ECNFs/CaP) in order to produce osteo-compatible nanofillers in epoxy resin as targets for bone repairing applications.

This particular type of nanofibers was produced with the electrospinning process, starting from a solution of polyacrylonitrile and CaP precursor sol-gel, followed by peroxidation and carbonization. Long and continuous nanofibers were fabricated; then, they were ultrasonically chopped, mixed into epoxy resin and cured.

CaP nanoparticles endow ECNFs with a rough surface that improve nanofibre-matrix interfacial adhesion through mechanical interlocking mechanism and, in addition to that, they provide satisfying calcium and phosphate ion release behaviour which is fundamental for bone remodelling. After that, a comparison with pure CNFs, undergone to a similar ultrasonication treatment, was made.

The strong fibre–resin bonding led to significant improvement in flexural strength and modulus of the resultant epoxy composites compared to pristine ECNFs, which suggested that CNF/CaP is a promising reinforcement for bone repairing materials.

One of the most important field where nanofibers are widely and efficiently employed is the fabrication of polymer composite laminates, in order to increase fracture toughness [18].

In fibre reinforced polymers (FRP), a number of layers of prepregs (combination of semi-cured resin and fibre reinforcing filler) are assembled together in order to obtain a composite laminate; fibre fabrics dominate in-plane mechanical properties (typically high), whereas resin matrices dominate out-of-plane mechanical properties (interlaminar shear strength, delamination toughness) which are generally lower than in-plane properties.

Given that the most common and critical failure mode in composite laminates is delamination, which consists in the separation of the different layers of which the composite is made of, it is really dangerous because, the failure starts and proceeds under the material surface and so it is usually undetectable from the outside.

Therefore, it has been necessary to find additional reinforcing agents to be incorporated between laminae in order to improve out-of-plane properties of the composite laminates. Carbon nanotubes and nano clay have attracted a lot of attention, as well as nanofibers.

Wu et al [22] found that a particular kind of self-healing core-shell nanofibers fabricated by co-electrospinning between dicyclopentadiene (DCPD) are used as the healing agent and PAN as the enwrapping agent. These nanofibers were incorporated at the interface of carbon-fibre fabrics, as it is clear from Figure 19, before resin infusion and then formed into self-healing interlayers after resin infusion and curing.

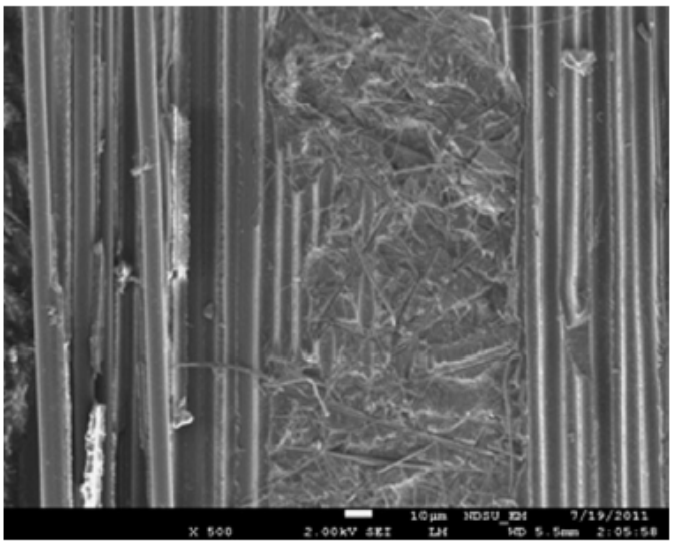

Figure 19 - SEM micrograph of the cross-sectional area of a nanofibre interlayer in a UD carbon-fibre reinforced PMC [22].

The production process is composed by two steps: the first is based on wet prepreg layup using vacuum bag compressive moulding with the aid of a hot press (which guarantees the uniform wetting of the nanofibers into resin), followed by a VARTM technique step.

A three-point bending test was used in order to evaluate the self-healing effect of the core-shell nanofibers on the flexural stiffness of the composite laminate after pre-damage failure. Promising results were achieved: the flexural stiffness after pre-damage failure can be completely restored using these new self-healing nanofibers; in

addition to this, it must be considered that the present technique has a very low weight penalty (<1% in volume fraction), as well as very low nanofibre content, a very low impact to the process and to the specific properties of the PMCs. The releasing of the healing agent and the toughening and self-healing mechanism of the core-shell nanofibers is confirmed by SEM micrographs reported in Figure 20.

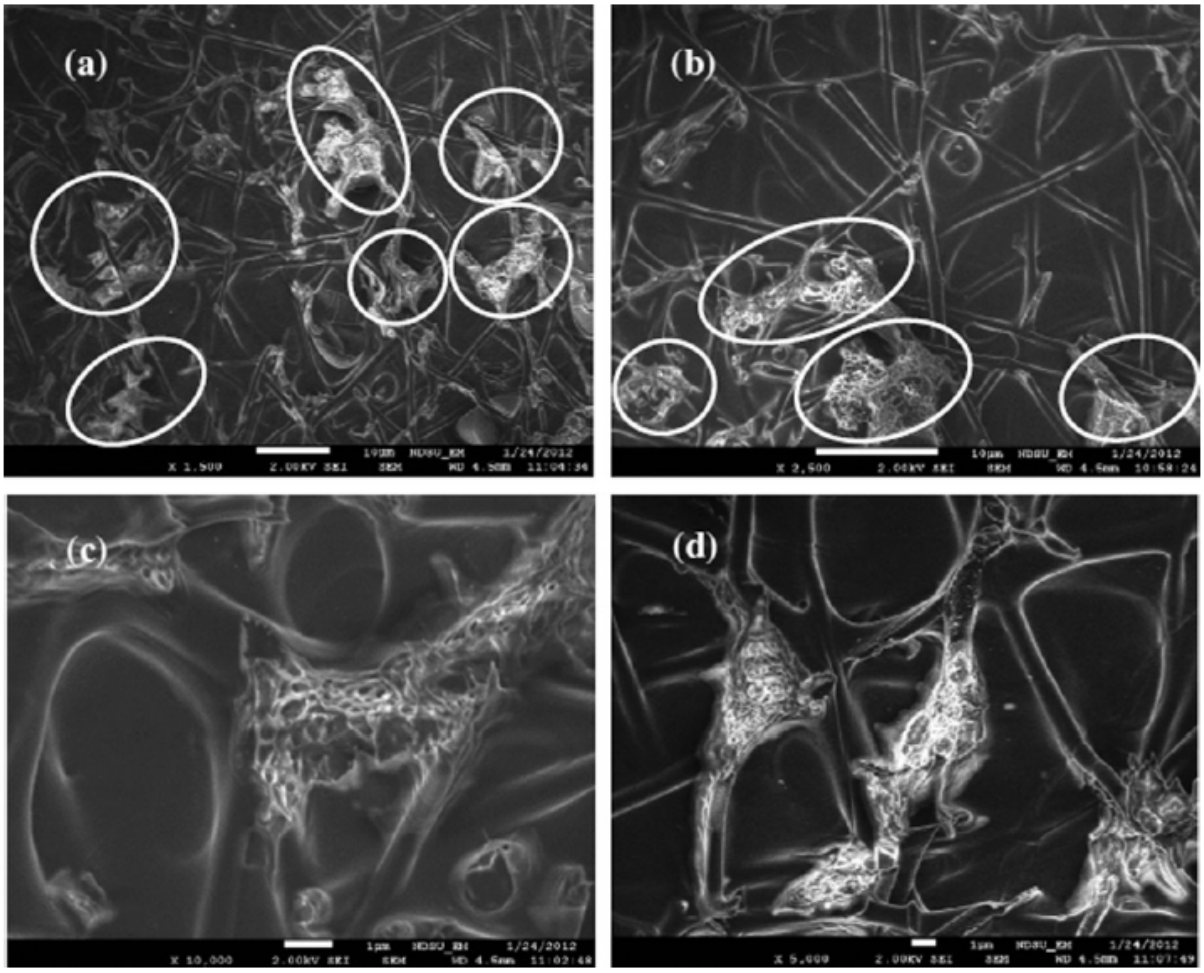

Figure 20 - SEM micrographs of failed surfaces of the hybrid multiscale self-healing PMC after three-point bending test (interfacial self-healing mechanisms). (a, b) Core-shell nanofibre networks (circled spots are the regions with autonomically released DCPD after pre-damage failure); (c, d) Delivery of healing-agent at core-shell nanofibre breakages due to interfacial and plastic failure of healed spots after post three-point bending test [22].

Such good results are really promising in particular for advanced applications such as aerospace, aeronautical and automotive.

The last application useful to report is the use of electrospun nanofibers as reinforcing fillers in epoxy adhesives with the purpose of the enhancement of mode I fracture toughness.

According to Musiari et al. [23], the use of an electrospun Nylon 6,6 nanofibrous mat was analysed as adhesive carrier and reinforcing web in adhesive bonding. In Figure 21 morphology of the nanofibrous mat adopted in this work are reported.

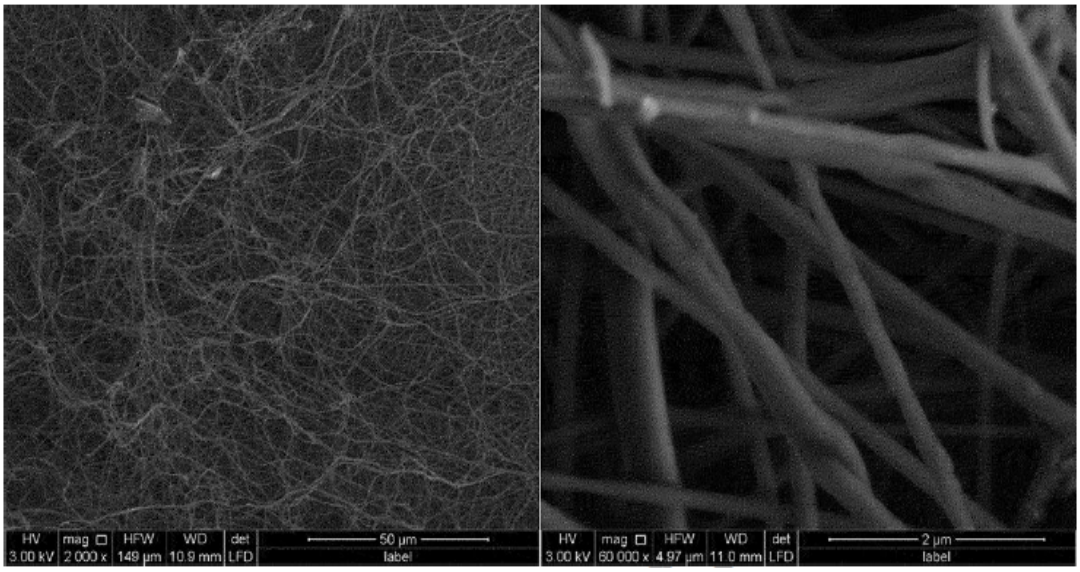

(a) (b)

Figure 21 - SEM images of the nanomat: 2000x (left); 60.000x (right) [23].

The solvent system used for the preparation of the electrospinning solution is a 1:1 volume ratio formic acid/chloroform solution with a concentration of Nylon 6,6 of 20% by weight. The adherends were obtained from a 2024-T3 aluminium plate.

After that, DCB tests on neat and nano-reinforced specimens were carried out and thank to them, an improving of the fracture toughness compared to the one of the neat resin was proven; the problem is that since the joints failed at the resin-adherend interface (adhesive fracture), the reinforcement could not be evaluated in absolute terms.

SEM analysis were done and the micrographs, reported in Figure 22 of the nano-reinforced specimens revealed the presence of nanofibers attached to the adherend surface; furthermore, nanofibers resulted stretched during the crack propagation: this could be associated to a crack bridging mechanism and to the enhancement of fracture toughness even though the crack did not run in the middle of the adhesive layer (cohesive fracture).

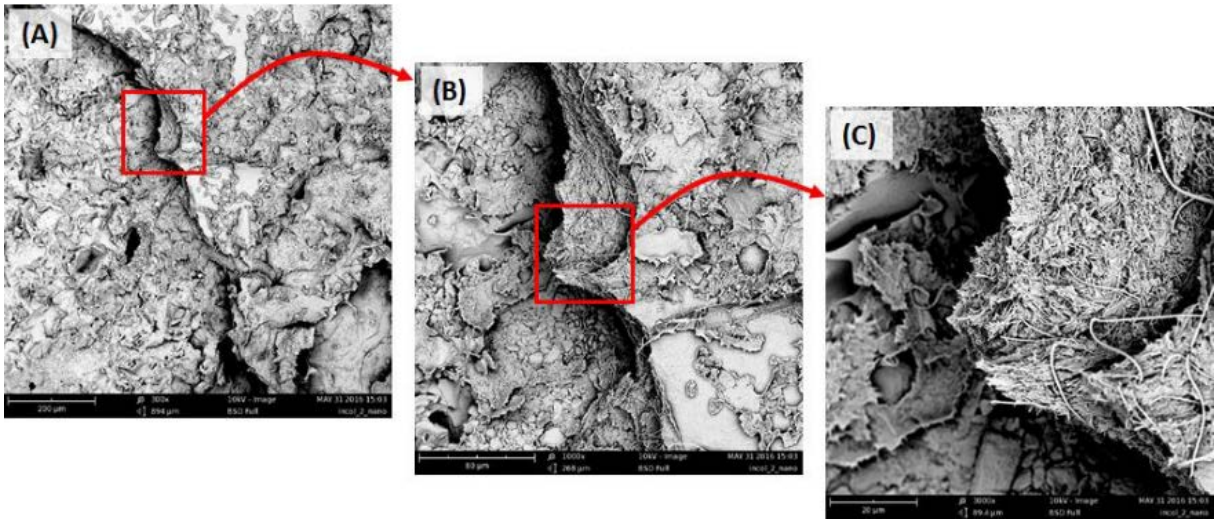

Figure 22 - SEM images of the fractured surface of a nanomodified specimen; (A) general view of the adhesive fracture surface at 100x magnification, (B) at 1000x magnification) and (C) at 3000x magnification [22].

The deviation of the crack path is attributed to the surface roughness: as a matter of fact, sandblasting, as well as helping resin to stick to the adherend, it may generates pockets of neat resin on the surface where the crack can run and cause a decrease of fracture toughness.

A development of the previous article is reported in [24] by Brugo et al., whose aim is to develop a laboratory route to add an electrospun polymeric nanomat to a two-part epoxy adhesive joint. The electrospinning solution is the same reported in [23], as well as the adherends material (2024-T3 aluminium plate).

Adherends were chemically etched in order to improve their wettability; full wetting is obtained when the nanomat, immersed into the adhesive for a few minutes, turns transparent when exposed to light.

After the preparation of the impregnated nanomat, it is used to bond the two adherends.

After curing, three different pre-cracking procedures were applied, in order to evaluate which was the best: fatigue pre-cracking, razor blade tapping and nanomat exfoliation. DCB tests were performed and they revealed that the nanomodified joint exhibits a force peak comparable or even lower than that of the virgin one, but the force during the propagation phase is higher (almost twice) and the decrease is smoother. In the first millimetres of the nano-reinforced joint, the crack runs close to the surface (adhesive fracture, probably caused by a small quantity of adhesive which was not

expelled during bag vacuum curing); as it goes on, areas of cohesive fracture appear, which may be the reason for the increase of fracture toughness.
The effectiveness of this technique in improving the fracture toughness of the neat resin was proven but a better control on the vacuum bag consolidation is necessary in order to completely demonstrate the potential of nanofibrous reinforcement.

1.5 Production of nanofibers

In recent years, several processing techniques have been used to prepare polymer nanofibers [25]. The main are:

- *Drawing*: is a process that requires a highly viscoelastic material to undergo strong deformations but at the same time being cohesive enough to support the stresses developed during the pulling. After the pulling, solidification occurs, in order to transform the spinning material in a single solid fibre [26].
  The basic setup of the fibre-drawing production method is reported in Figure 23:

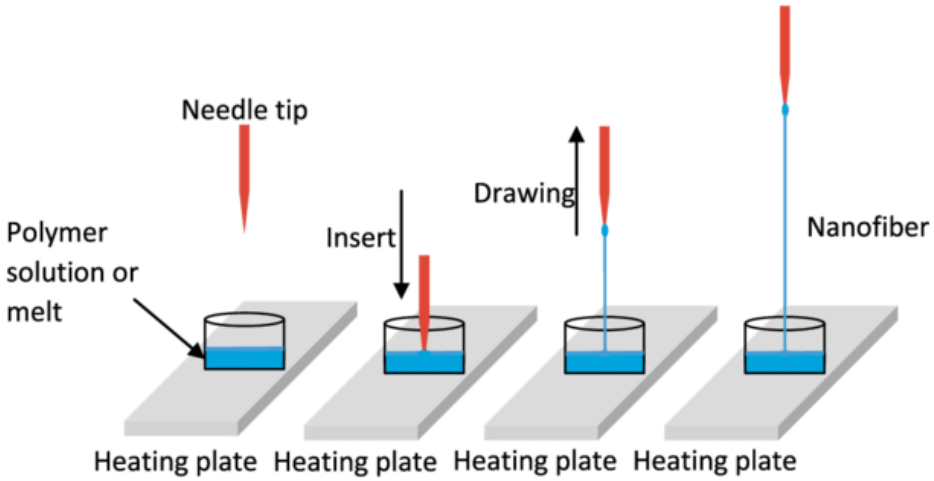

Figure 23 – Nano-fibres drawing process [27].

- *Template synthesis*: is a process that uses a nano-porous membrane as a template, as shown in Figure 24. The solution is extruded through the nanometric-size holes in the membrane and this allows to control the diameter of the nanofibers by choosing the diameters of these holes [28]. Fibrils and tubule can be manufactured, but one-by-one continuous nanofibers cannot.

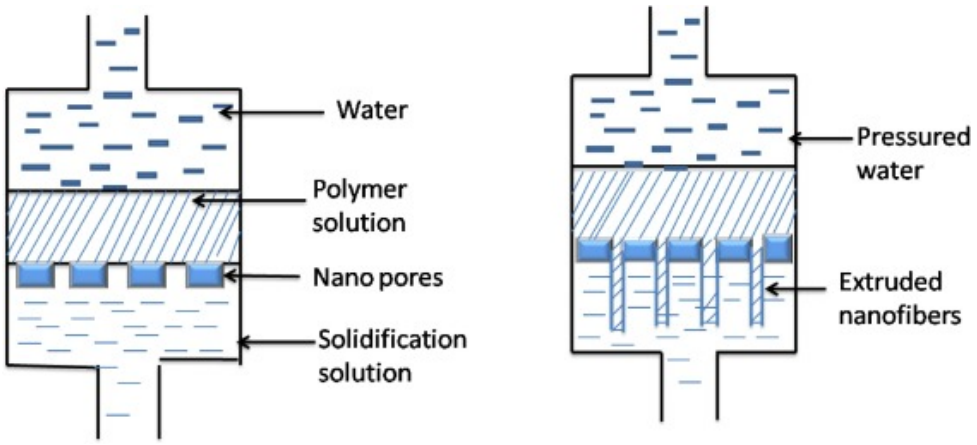

Figure 24 - Nanofibers template synthesis process [29].

- *Phase separation:* the fundamental steps of this process consists of dissolution, gelation, extraction using a different solvent, freezing and drying, resulting in a nanoscale porous foam. The gelation step generates phase separation due to the incompatibility of the component's phases in the solution. Once the gelation is finished, nanofibers are extracted [28].
  A simplification of the phase separation process is described in Figure 25.

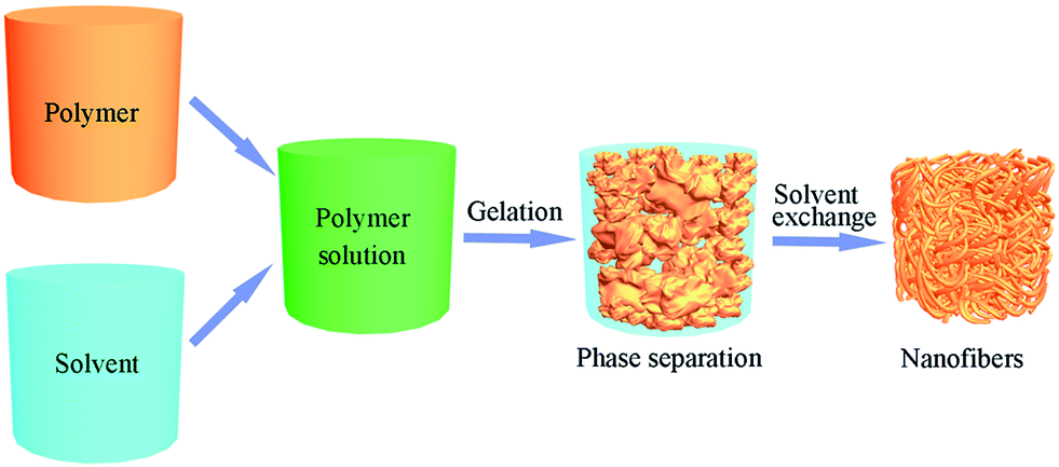

Figure 25– Phase separation of nanofibers [30].

- *Self-assembly*: is a process that consists in an automatic disposition of nanofibers (or structured filaments, as displayed in Figure 26), along a predefined direction, by adding chemical reactants to the starting solution. Often this process takes place thank to opposite polarity present in one molecule (hydrophobic tails, hydrophilic heads;).
  Like the phase separation, this technique is time-consuming in processing continuous polymer nanofibers.

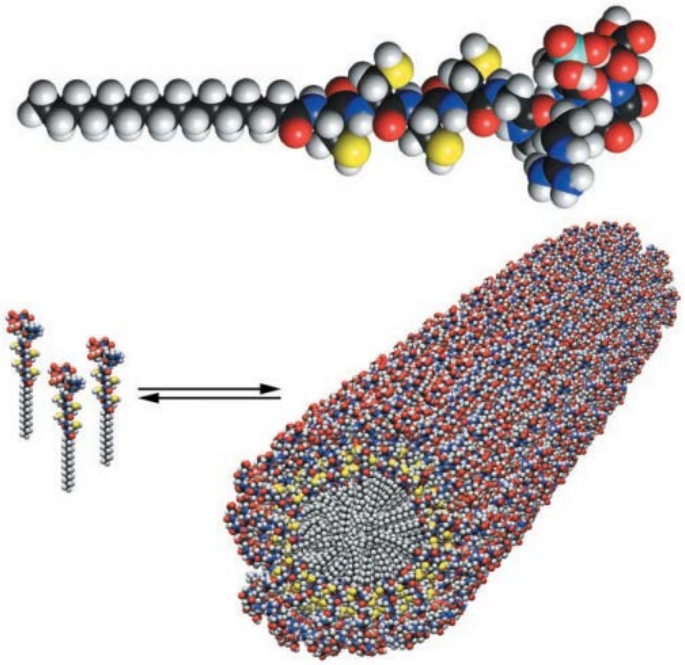

Figure 26 - Formation of nanofibers by self-assembly [31].

- *Electrospinning*: this technique is the one used in the present work for the nanofibers production so it will be extensively described in the next Section.

1.6 Electrospinning process

After the description of the electrospinning process, in Section 1.6.1 all the fundamental parts of the electrospinning apparatus are examined while in Section 1.6.2 process parameters are analysed.

The process starts with the polymer solution pushed inside the syringe through the needle thank to a pump; at the tip of the needle, where the intensity of the applied electric field increases, the solution drop tends to elongate (stretched by the difference of the electric potential between the two electrodes) generating a conical shape known as Taylor cone.
When the electrical field reaches a level where the repulsive electrical forces exceed the surface tension of the drop, a polymeric jet is ejected from the needle. In the space between needle and the collector, the solvent evaporates, and the charged polymer is deposited on the collector in the form of mat of nanofibers.
A schematization of electrospinning process is reported in Figure 27.

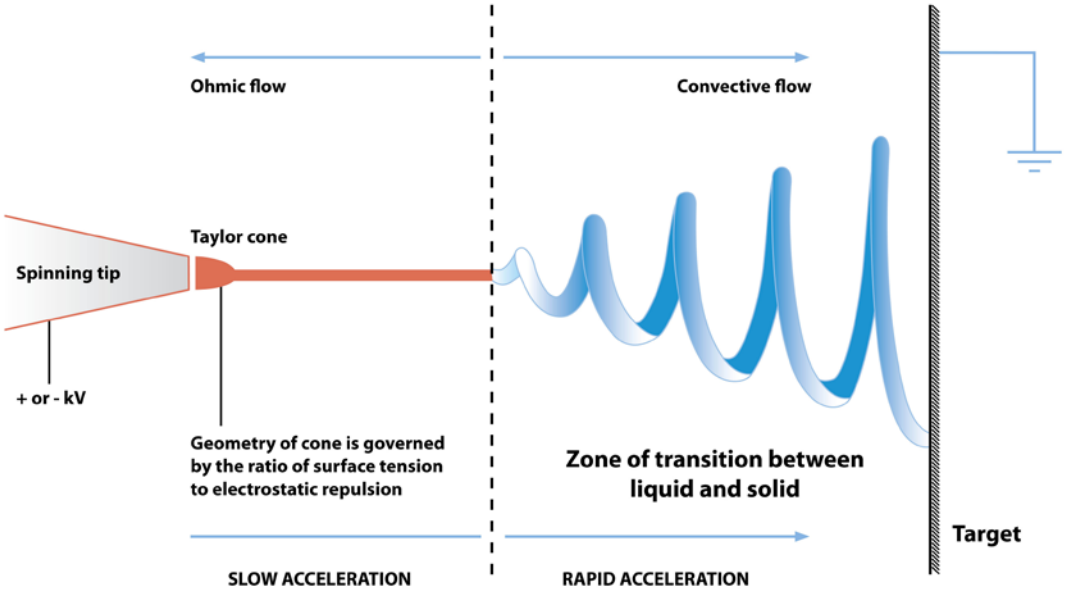

Figure 27 - Nanofibers formation with electrospinning process.

1.6.1 Parts of the electrospinning apparatus

The fundamental components of the electrospinning apparatus [32] are three:

- *High voltage generator*: it is directly connected to the needles (which act then as electrodes) and it conducts the charge to the polymer solution.

- *Pumping system*: it is made of one or more syringes filled with the polymer solution. On the top of each syringe there is a needle, with a hole of calibrated diameter, to which is connected the high voltage generator.

- *Collector*: it is made of metal and it is generally connected to ground. It may come in different shapes such as plate or rotating cylinder.

1.6.2 Electrospinning parameters

Different parameters come into play; some of them with regard to the polymer solution, others in connection with the process and the apparatus; they all have a fundamental role for what concerns the morphology and diameter of the electrospun nanofibers [28][32][33].

Solution parameters

- *Concentration of polymer*: it plays an important role, both for the aspect of nanofibers (diameter and morphology) and for their properties.
  Four critical concentration exist [28] [33]:
  1. With a very low polymer concentration, electrospray process occurs instead of electrospinning one; in addition, nano particles are formed instead of nanofibers.
  2. Little higher concentration generates a mixture of beads and fibres.
  3. With a consistent concentration, smooth nanofibers can be obtained.
  4. If the concentration is very high, instead of nanofibers, helix-shaped micro- ribbons will be generated; this structures' diameter is bigger than nanofibers.

  In Figure 28 the four different nanofibers morphologies corresponding to the four different concentrations reported above are reported.

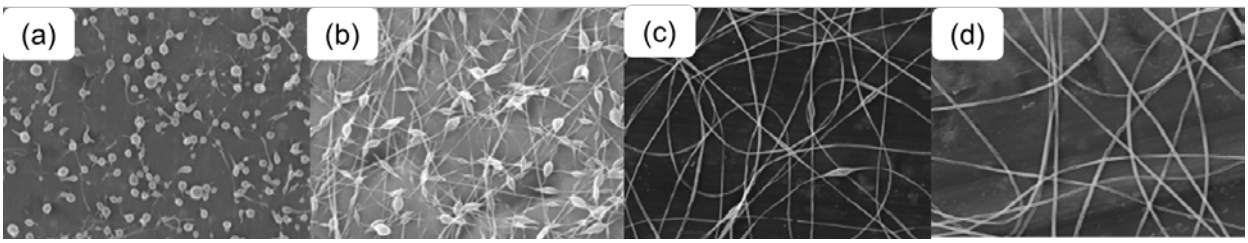

Figure 28 – Four different nanofibers morphologies corresponding to the four concentrations described above: (a) very low concentration, (b) low concentration, (c) right concentration and (d) high concentration [34].

Obviously, the higher is the polymer concentration, the higher will be the viscosity of the solution.

- *Viscosity*: it is the critical key in determining fibre morphology and diameter.
  If viscosity is too high, ejection from the needle becomes more difficult, if it is too low, fibres with beads will be obtained.

- *Molecular weight*: directly connected to viscosity (higher molecular weight leads to higher viscosity). In addition, if the concentration of the polymer is fixed, a low molecular weight will lead to beads rather than smooth nanofibers.

- *Surface tension*: it is an important factor for what concerns final morphology of the nanofibers. Fixing the polymer concentration, a reduction on the surface tension of the solution can transform beaded fibres into smooth fibres; a way to decrease surface tension is to use a solvent/solvent mixture with a lower surface tension or by using a surfactant.

- *Electric conductivity of the solution*: the fibre diameter decreases with increasing of conductivity. If the conductivity is low (e.g. natural polymers), it can be increased with the help of ionic salts.

- *Vapour pressure*: it is important because it may cause problems with solvent evaporation before and during spinning. At the same time, a wrong value of surface tension may influence the formation of non-cylindrical morphologies.

Process parameters

- *Voltage*: the electrospinning process takes place only when the applied voltage is higher than the threshold voltage, in order to charge at a sufficient level the polymer solution ejected from the Taylor cone. Basically, a higher applied voltage (so a higher applied force) leads to a smaller diameter of the fibres.

- *Distance between collector and spinneret*: if the distance between the two is too small, evaporation of the solvent does not fully occur; if the distance is too big, fibres with beads will be obtained.

- *Flow rate*: it is the rate with which the solution ejects from the needle, thanks to a pump. Lower flow rate allows for a better degree of polarization of the polymer solution; if the rate is too small it may cause a non-constant jet of nanofibers from the needle and then a stop in the Taylor cone developing. Instead, if the flow rate is too high it may provide a pulsing jet and bead fibres instead of smooth ones.

Surrounding conditions

- *Temperature*: it has an effect directly on the viscosity of the solution; higher temperature causes a decrease of viscosity and so smaller fibre diameter will be obtained.

- *Humidity*: it is of the key factor and it must be always controlled accurately. In principle, the degree of humidity must be kept low in order to facilitate solvent evaporation; indeed, high humidity will generate a thicker diameter of the fibre and it may make solvent evaporation harder.

1.7 Adherends surface pre-treatments

After analysing advantages and disadvantages of the use of adhesive, a further chapter is needed in order to describe one of the key factors in the world of adhesive: surface pre-treatments to enhance adhesion. In this work, a study on aluminium adherends and their pre-treatments has been performed.

In the last 30 years, the employment of bonded aluminium has become more and more important, in particular in aerospace, transport and general engineering industries.

For what concerns aluminium, surface treatments can be divided into the following different groups [35]:

Mechanical treatments

- *Abrasion*: grit-blasting or sandblasting use graded alumina or silica to produce a highly macro-rough surface and to remove the oxide layer from the aluminium surface in order to allow mechanical interlocking adhesion process. Sandpaper can be used too. Scotchbrite and wire wool bring poorer wettability results in comparison with the methods listed above.

- *Degreasing*: it can be distinguished between liquid and vapour degreasing and it is carried out in order to remove oils and other organic contaminants which can be present on a mill-finished surface.

  Generally, it is the first stage of the majority of multi-stage treatments.

  Examples are rinsing or wiping with acetone, methyl ethyl ketone, isopropyl alcohol.

- *Corona discharge treatment*: the aim of this technique is to increase the surface energy. The durability is poor because a weakly-bound oxide is believed to form and to be the cause of this poor durability.

- *Plasma-spray coating*: 99.5% pure alumina powder plasma sprayed onto a mechanically roughened surface has been shown to facilitate good adhesion in glass reinforced epoxide composite to aluminium joints [35].

Chemical treatments

- *Alkaline cleaning*: the specimen is immersed in an alkaline solution in order to remove organic contamination (oil or machining lubricants). Commonly, just like degreasing, it is the first step of multi-stage treatments. The reaction that occurs is the following, as reported by Chatterjee et al. in [36]:

  (1) $2Al + 2NaOH + 2H_2O \rightarrow 2NaAlO_2 + 3H_2$
  (2) $2NaAlO_2 + 4H_2O \rightarrow 2Al(OH)_3 + NaOH$

  The two combined give:

  (3) $2Al + 6H_2O \rightarrow 2Al(OH)_3 + 3H_2$

- *Chromic acid etching (CAE)*: there are a lot of different CAE techniques. The most common and used is the “optimized FPL etching” or simply FPL etch (FPL: Forrest Products Limited, from the inventors of the process).
  The reaction that occurs is the following [37]:

  (1) $2Al + H_2SO_4 + Na_2Cr_2O_7 \rightarrow Al_2O_3 + Na_2SO_4 + Cr_2SO_4 + 4H_2O$

  The aluminium oxide formed in the previous equation is dissolved by the reaction with sulfuric acid as shown in the following equation:

  (2) $Al_2O_3 + 3H_2SO_4 \rightarrow Al_2(SO_4)_3 + 3H_2O$

The reaction (1) proceeds faster than reaction (2), leaving a controlled amount of Al_2O_3 on the surface.

A recent improvement of this technique consists in adding the aluminium alloy 2024-T3 (rich in copper) in the etch solution; copper ions seems to help the formation of small deep pores on the surface and the outcome of this is the development of a better surface for bonding.

After the immersion in the etching solution, rinsing is a crucial step: drying before the surface is completely rinsed must be avoided.

A scheme of how the surface looks like after treatment is reported in Figure 29.

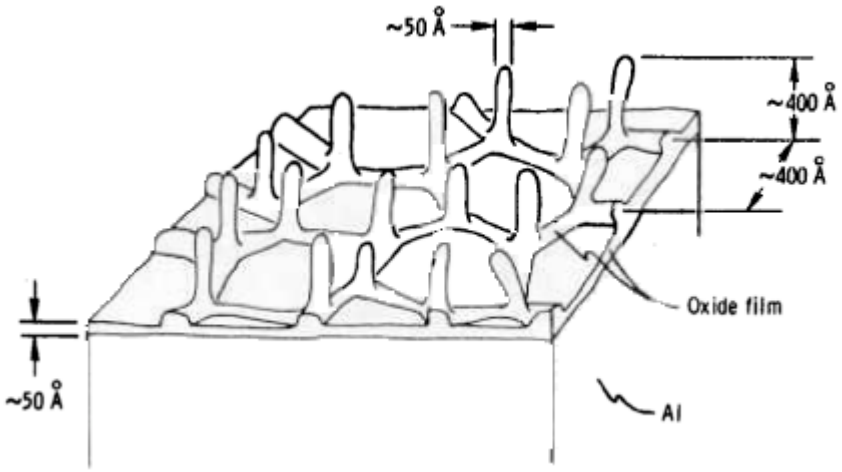

Figure 29 - Isometric drawing of oxide structure [37].

- *P2 etch process*: it is a process with minimal toxicity that has been developed in order to substitute chromic acid etching (chromate ion is carcinogenic).

  This etchant contains 370 g of concentrated sulfuric acid, 150 gr of 75% ferric sulphate, and sufficient water to produce 1 L of the etchant [37].

  It provides rough surfaces suitable for adhesive bonding; they are better than those obtained with abrasion because in this case they are nanostructured and thus the strengths of the resulting joints are similar to those produced with FPL etch.

  These are the main reasons why, in the present thesis, P2 etch will be the only surface treatment used for our aluminium specimens.

(1) $2Al + 6H^+ \rightarrow 2Al^{3+} + 3H_2$

(2) $Cu + 4H^+ + SO_4^{2-} \rightarrow Cu^{2+} + SO_2 + H_2O$

Equation (1) represents the standard attack on aluminium by acids.
Equation (2) represents the action of hot sulfuric acid as an oxidising agent towards copper.

(3) $3Fe^{3+} + Al \rightarrow Al^{3+} + 3Fe^{2+}$
(4) $2Fe^{3+} + Cu \rightarrow 2Fe^{2+} + Cu^{2+}$

Equation (3) reports the fact that ferric ions are corrosive to aluminium, while equation (4) points out that the same ions attack copper. It is clear that the use of sulfuric acid alone would have a less significant effect with regard to P2 etch, in which ferric salts are used.

Electrochemical treatments

- *Chromic acid anodising (CAA)*: it is an electrochemical process that leads to the formation of a thick (1.5 - 3μm) aluminium basic oxide film by rapidly controlling the oxidation of an aluminium surface; in particular, the porous surface structure (Al_2O_3) is converted to $Al(OH)_3$. The resulting aluminium oxide film is electrically non-conductive and, in addition to that, it is usually not suitable for adhesive ; to solve this problem, chromic acid is added to the seal water in order to let it dissolve part of the cell structure and to leave a thick and strong layer of aluminium oxide, to which adhesive could form durable bonds [37].

- *Phosphoric acid anodising (PAA)*: it is the preferred treatment of the Boeing Aerospace Company [38]. It generates a thick (400 – 800nm) oxide layer, including small protruding fibrils of 100nm. The presence of phosphate ions gives to the oxide excellent moisture-resistant characteristics [35].
  No significant differences in terms of lap shear strength were pointed out between FPL etch, the P2 etch, the PAA process or the CAA process [37].

1.8 Double Cantilever Beam Test

Different methods to evaluate fracture toughness are available: in Figure 30 mode I, mode II and mode III fracture modes are exemplified.

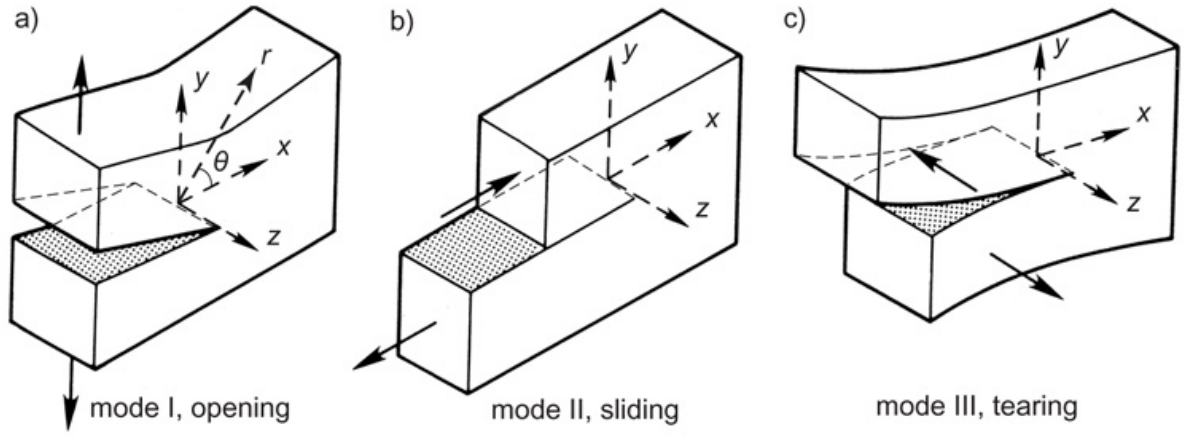

Figure 30 – Different fracture modes: a) opening, b) sliding and c) tearing [39].

The present work will be focused only on mode I fracture, evaluated with DCB test, given that adhesives suffer mainly from this type of fracture caused primarily by edge effects.

DCB is a standard test that allows to obtain the mode I fracture energy of adhesive bonds; in this work ASTM 3433 was adopted as a reference [40].

This standard provides the guidelines for DCB metallic specimens, starting from the production process of the adherends up to the complete test setup.

The first step is the creation of an initial crack between the metallic adherends by inserting a wedge, before the curing process of the adhesive. After curing, specimens are placed on the fixtures of the testing machine and loaded until failure. Finally, the test is stopped. During the test, displacement, load and crack propagation are measured and recorded.

The ASTM method allows calculation of the value of the fracture toughness on the basis of elastic stress analysis and hold for a sharp-crack condition under severe tensile restrictions. It is assumed that the plastic region of the crack-tip is small if compared with the size of the crack.

The fracture toughness is computed for the initiation of the crack, where the load is maximum, and for the moment when the crack propagation stops (arrest load) [28]:

$$G_{Ic} = \frac{[4L^2(\max)][3a^2 + h^2]}{EB^2h^3}$$

$$G_{Ia} = \frac{[4L^2(\min)][3a^2 + h^2]}{EB^2h^3}$$

Unit of measure: [J/m^2]

where:

- G_{Ic}: Fracture toughness from load to start crack
- G_{Ia}: Fracture toughness from arrest load
- L (max): Load to start crack (N)
- L (min): Load at which load stops growing (N)
- a: Crack length (mm)
- h: Thickness of adherends (mm)
- B: Specimen width (mm)
- E: Tensile modulus of adherend (MPa)

In addition to the displacement value acquired by the instrument, a clip-gage has been installed in order to evaluate the Crack Mouth Opening Displacement (CMOD), δ'. CMOD measures the resistance of a material to the propagation of a crack and it is used on materials that can show some plastic deformation before failure occurs that causes the tip to stretch open [41]. Two measures are necessary because the instrument considers the deformation of the test driveline only, while clip gage evaluates the real specimen dislacement. The crack length is calculated from the specimen compliance using a beam on elastic foundation concept that considers the out of plane deformation of the adhesive layer and the rotation at the crack tip, modified to account for the distance of the CMOD measurement point from the loading axis and for the effect of shear on the deformation of the cantilever [42].

$$\frac{\delta'}{P} = 2\left[\frac{2\lambda_\sigma}{k}(1 + \lambda_\sigma a) + (a + g)\frac{2\lambda_\sigma{}^2}{k}(1 + 2\lambda_\sigma a) + \frac{a^3}{3EJ} + g\frac{a^2}{2EJ}\right]$$

where λ_σ and k are:

$$\lambda_\sigma = \sqrt[4]{\frac{6}{h^3 t}\frac{E_a}{E\left(1-\nu_a^2\right)}}$$

$$k = \frac{2b}{t}\frac{E_a}{\left(1-{\nu_a}^2\right)}$$

In Figure 31 a scheme of the standard flat adherend specimen is reported.

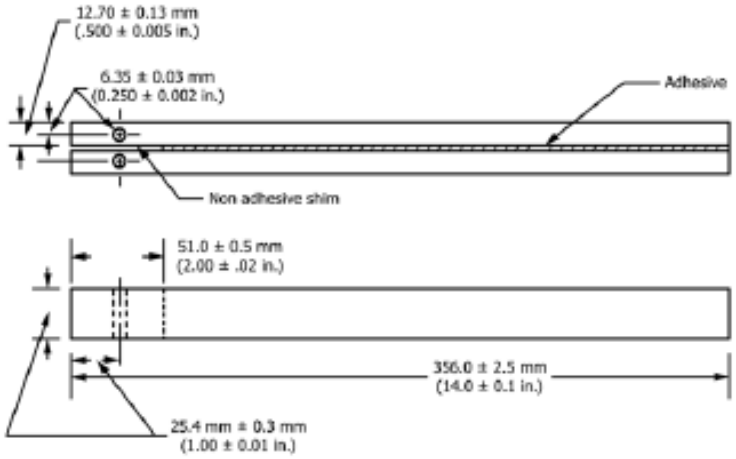

Figure 31 – Flat adherend specimen suggested by ASTM 3433 standard.

The strain energy release rate G is:

$$G = \frac{P^2 a^2}{bEJ}\left(1+\frac{1}{\lambda_\sigma a}\right)^2$$

In Figure 32, the specimen setup during a DCB testing is reported.

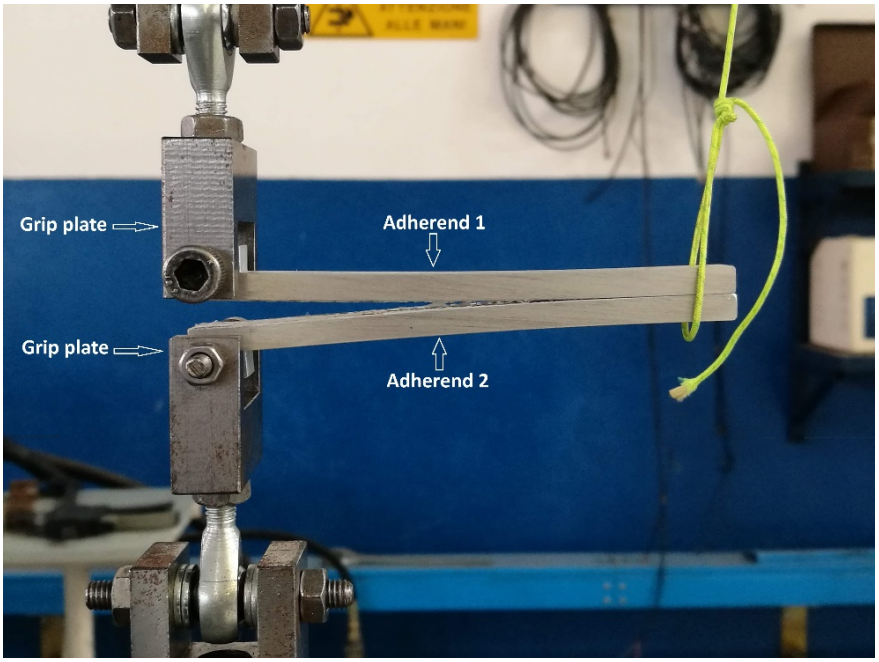

Figure 32 – DCB test configuration.

2. AIM OF THE THESIS

The main aim of the present work is to increase mode I fracture toughness of adhesive bonded joints, by means of electrospun Nylon 6,6 nanofibers in an epoxy matrix. To achieve that, different parameters will be investigated, in order to obtain an optimal adhesion between the aluminium adherends, such as:

- *The nanofibers*: introduction of nanofibers as reinforcing fillers for adhesive is a technique that has been developed in recent years. Polymers nanofibers provide a large surface area to volume ratio, flexibility and lend better mechanical performances to the adhesive. A literature review will be done in order to analyse also other types of nano-reinforcing fillers and the effects of their application, in particular on mechanical properties.
- *The resin*: the adhesive used to perform adhesion is an epoxy resin provided by ELANTAS. An accurate method for the preparation of the adhesive will be developed, in order to solve one of the most crucial problems, that is the formation of bubbles that causes preferential path for crack propagation. In addition to that, production of a nanofibrous prepreg has also been attempted; hence, a method to enhance impregnation and to calibrate the thickness of the prepreg has been developed, in order to avoid resin surplus.
- *The surface pre-treatments*: one of the most important requirements to obtain high bonding strength and durability is an accurate preparation of the specimen surface. In the present work two different pre-treatments will be investigated: mechanical (abrasion) and chemical (basic pickling and acid etching). A surface preparation method will be developed in order to try to obtain the best condition for adhesive bonding.

Those parameters will be experimentally studied: aluminium specimens will be produced, treated with optimized surface pre-treatments, bonded (with neat and nano-reinforced resin) and then tested with a mode I fracture test called DCB (Double Cantilever Beam). DCB test consists in the application of a tension force perpendicular to both bonded substrates; the crack of the joint will be obtained, and the fracture toughness will be measured. At this point, aluminium surfaces will be visually observed and SEM analysed in order to study the aspect of the fracture surface and provide some conclusions to the studies carried out.

3. RESULTS AND DISCUSSION

In this Section, all the results of the present work are presented. In Section 3.1 results about the adhesive are discussed, in particular for what concerns bubble removal process, resin preparation method and DSC analyses on the resin. In Section 3.2, results concerning adherends surface preparation and the final treatment method are presented. In Section 3.3 are reported thickness measures of the cured joint and the methods to evaluate it, while in Section 3.4 DCB tests results both on virgin and nanomodified specimens are largely explained.

3.1 Epoxy adhesive

The epoxy resin selected for this work is the a bicomponent system; it is used for a wide range of different materials, showing an excellent resistance to peeling, it is solvent free and provides resilient bonding, having a high viscosity system.

3.1.1 Bubbles removal

As reported by Díaz Muñiz in [28] and Brugo in [24], the main problem with this adhesive is the presence of a substantial number of bubbles after curing, as it is clear from Figure 33.

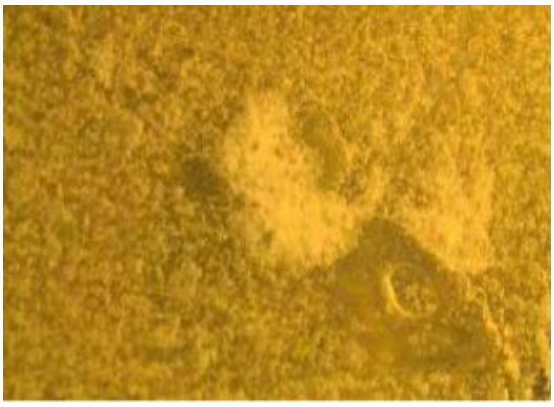

Figure 33 - Optical image of AS46/AW46 after curing [28].

So, the first aim of the internship was to find a way to remove bubbles, given that they act as defects and facilitate crack propagation, reducing bonding strength.
Different attempts were made in order to reach an almost-complete bubbles removal.
The starting step is always pouring resin and hardener into a plastic cup and gently mixing for 30 seconds until a mostly homogeneous system is obtained

1) In the first attempt, the plastic cup is put into a dessicator connected to a vacuum pump (see Figure 34); in this way bubbles are forced to go up to the surface.

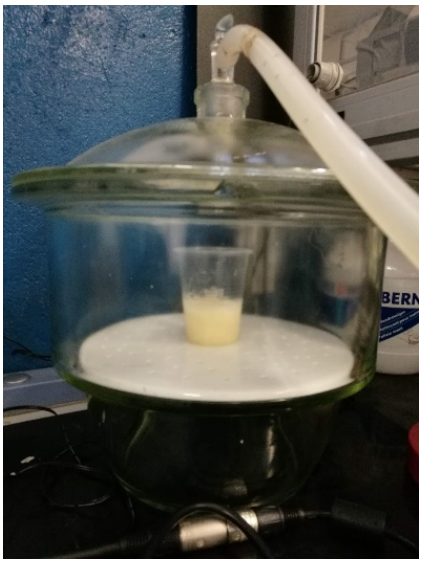

Figure 34 - Resin in a plastic cup put in a crystallizer under vacuum.

For the first cycle, the resin is put 10 minutes under vacuum and then the crystallizer is aerated (vacuum is removed); after that, the resin is poured into an aluminium machined template (previously treated with a release agent in order to be able to remove the cured resin easier). The second cycle is composed by two vacuum cycles alternated by aeration (and eventually up to four vacuum cycles).

Formation of a dense foam which contains the bubbles is observed; after the vacuum pump is switched off, the foam settles down. After the curing cycle, an important number of bubbles persists, regardless the number of vacuum cycles the resin is undergone.

2) In addition to the use of the vacuum, it is been taken into account the use of a 26KHz sonicator at its full power (200Watt) in order to try to crush all the little bubbles present in the bulk of the mixture and to emphasize the degassing effect of the vacuum.

As in the attempt above, up to four cycles of vacuum were made, each one alternated with aeration and 2 minutes of sonication (the tip of the sonicator is immersed in the resin, so obviously this step takes place with the crystallizer open).

Before the third cycle of sonication, a problem occurred: resin started curing inside the plastic cup as a result of the heat generated by the vibrations of the instrument.

3) After that, it is been tried to use the sonicator for 30 seconds instead of 2 minutes for each step and to reduce the cycle time (0.4 seconds of vibrations alternated with a pause of 0.6 seconds). In this way, the quantity of heat provided to the resin is definitely lower: the resin doesn't start curing, but a high number of microscopic bubbles started growing in the bulk of the mixture (it is easily observed when the resin is poured into the template).
   It can be concluded that sonicator suppresses bigger bubbles, but generating an excessive number of micro-bubbles; the problem persists.

4) A further development of the previous two points is the use of a little hole on the bottom of the plastic cup, from where the resin will be poured instead of tilting the cup and pouring from the top. Theoretically, bubbles tend to rise to the surface and, pouring from the bottom, would have led to a lower number of bubbles in the template; in practice there are too many micro-bubbles in the bulk, so this expedient ends up being useless for this application, but not in general, thus it will be used in all the following attempts.

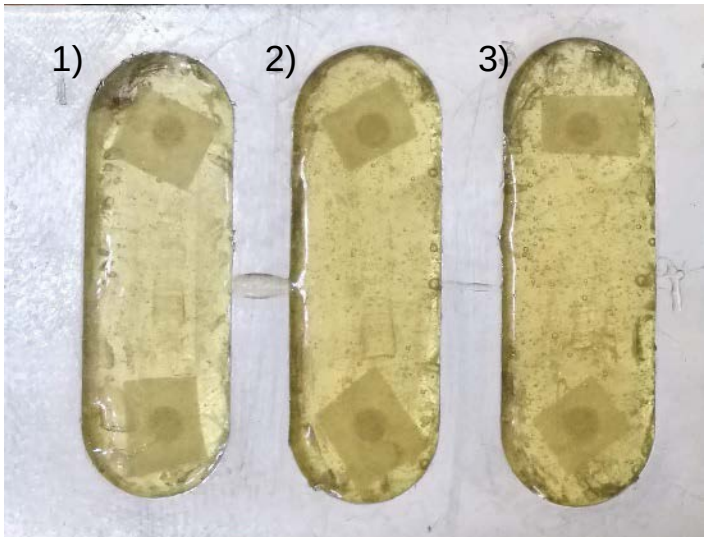

Figure 35 - Resin after curing: 1) one vacuum + sonication cycle; 2) two vacuum + sonication cycle; 3) three vacuum + sonication cycle.

Observing Figure 35 reported above, it is clear that the more sonication is used, the more the number of micro-bubbles increases.

From now on, pouring will always take place from the hole in the bottom of the cup, made before the preparation of the resin/hardener mixture and sealed with simple paper tape.

5) In order to try to remove micro-bubbles on the surface, the use of a blowtorch, with the aim to burn oxygen contained into them, was introduced. So, after up to four cycle of vacuum and sonication (carried out as described in 3)), flaming was used for 10 seconds on the uncured resin, so that the end of the flame reached the surface of the specimen. Obviously, the flame was not left static on a single point, but it was moved all over the surface.
   Not satisfying results were achieved, with only a little part of the bubbles removed; so, flaming was abandoned, also because it has another aggravating aspect: it could lead to localized curing of the resin. In Figure 36, a comparison between resin with and without surface flaming is reported.

Figure 36 - Resin after curing: 1) one vacuum + sonication cycle; 2) two vacuum + sonication cycle; 3) three vacuum + sonication cycle; 4) four vacuum + sonication cycle; 5), 6), 7) and 8) underwent flaming in addition to the cited-above treatment.

6) Another sonication procedure was introduced in order to avoid direct contact between the vibrating tip and the resin.
   The plastic cup containing the resin was immersed in a plastic bowl filled with water; sonication was set at maximum power and continuous vibration and the tip of the sonicator was put into the water.
   Anyway, not even this method led to bubbles removal.

7) Remaining convinced that some kind of slow mixing is necessary in order to obtain a complete resin degassing, a homemade battery mixer was assembled so that it is possible to put it inside the crystallizer. Continuous mixing under vacuum is fundamental because helps breaking all bubbles and avoid the formation of a gel glaze on the resin surface, allowing the expulsion of bubbles. Figure 37 (a) shows the homemade battery mixer while Figure 37 (b) exhibits the setup inside the crystallizer.

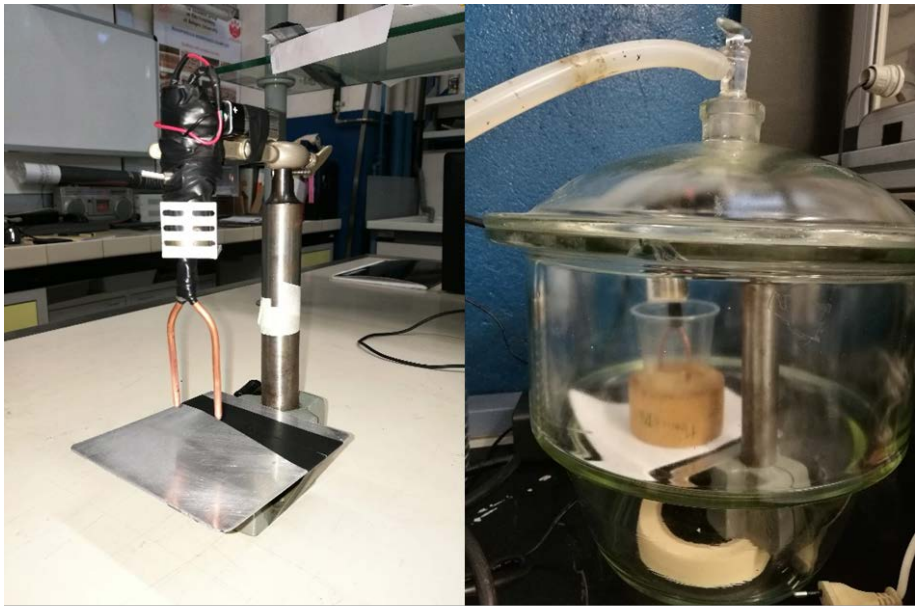

(a) (b)

Figure 37 – (a) Assembled battery stirrer and (b) Battery stirrer on a support inside the dessicator.

A single vacuum cycle of 10 minutes is carried out; the result is absolutely satisfying. As it is clear from Figure 38, the resin is almost devoid of bubbles and it is completely homogeneous.

During the application of vacuum, a dense foam is formed but it vanishes in 5-6 minutes time; this suggests that resin is completely degassed.

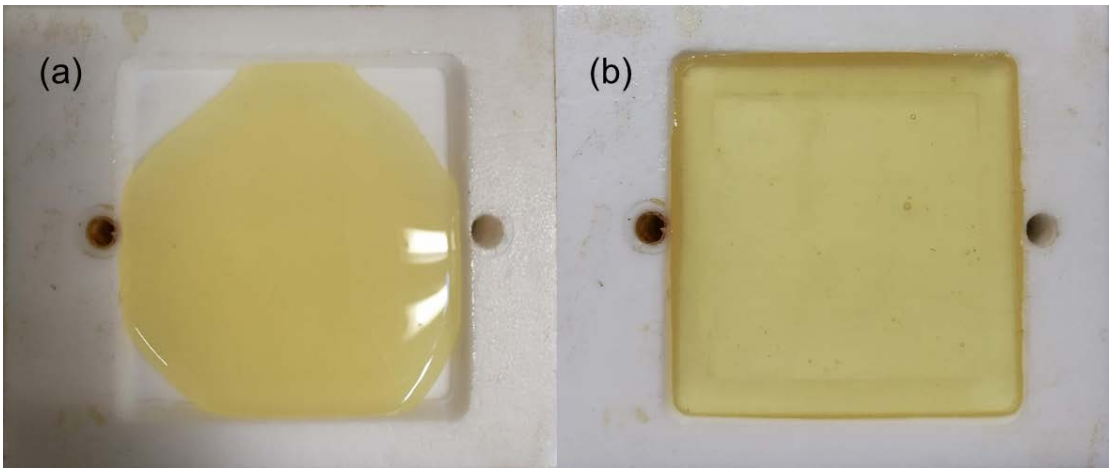

Figure 38 – (a) Uncured resin poured in a PTFE template and (b) Resin after curing process.

3.1.2 Optimized resin preparation method

1) After taking a plastic cup, a hole in the bottom is made using a cutter and then it is sealed with paper tape;
2) The cup is placed on a technical balance where the needed quantity of pre-polymer is weighted and then the corresponding amount of hardener is added (following the w/w ratio suggested by the supplier);
3) A timer is started: it is important to always consider time because this adhesive system has a very short pot-life (approximately 40 minutes)
4) Pre-polymer and hardener are mixed manually and gently, in order to make the resin homogeneous and avoid the formation of bubbles;
5) The battery stirrer is immersed in the plastic cup containing the resin and all together they are put inside the crystallizer; vacuum is applied for 10 minutes. Vacuum decreases surface tension and allows bubbles in the lower part of the bulk to rise to the surface and being expelled from the resin, which will be completely bubbles-free.
6) At this point, the resin is ready to be poured from the bottom-hole, in order to avoid entrance of air and to leave some bubbles enter into the adhesive, remaining then on the surface.

3.1.3 DSC resin analyses

DSC analyses are done in order to evaluate if the curing cycle in the oven leads to a complete curing of the resin; in addition to this, tests were carried out to evaluate the T_g (also to compare it with the value indicated by the manufacturer on the datasheet). In conclusion, both cured and uncured resin are analysed with DSC.

Cured specimens

Different curing ramps were tested in order to evaluate if there were significant differences between them.

The manufacturer suggested the following curing method: 3 h at 50 °C, with which a T_g of 57-60 °C should be reached.

In order to confirm values from datasheet, resin cured in the oven following the suggested curing cycle is analysed with DSC; the method log is reported in 5.1.1.

Curing cycle (1):

- Start from room temperature (~30 min corresponding to mixing time);
- ramp of 0.5 °C/min until reaching a temperature of 50 °C;
- 3 hours at 50 °C;
- cooling inside the switched off oven.

As it is clear from the thermogram reported in Figure 39 (where the first analysis cycle is taken into account), T_g results to be lower (48°C). However, the stepwise transition is the only relevant feature in the thermogram, thus suggesting that the reaction proceeded up to relevantly high degree of curing.

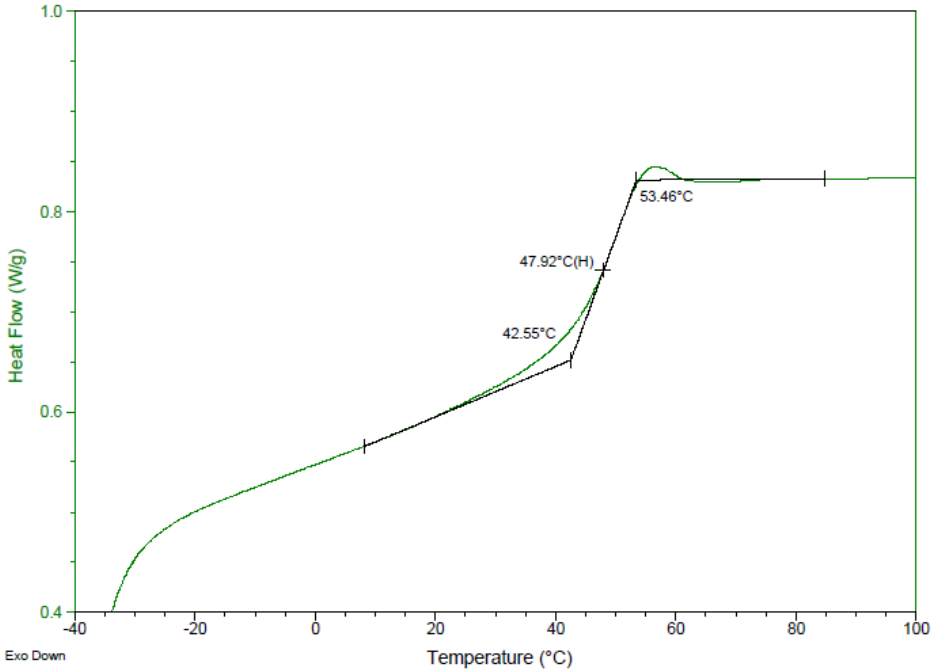

Figure 39 – DSC first cycle thermogram of specimen cured with cycle (1).

After that, also the second DSC cycle is elaborated (Figure 40) and results are compared with the first one, in order to verify if the curing process occurred in the oven lead to a complete curing of the resin.

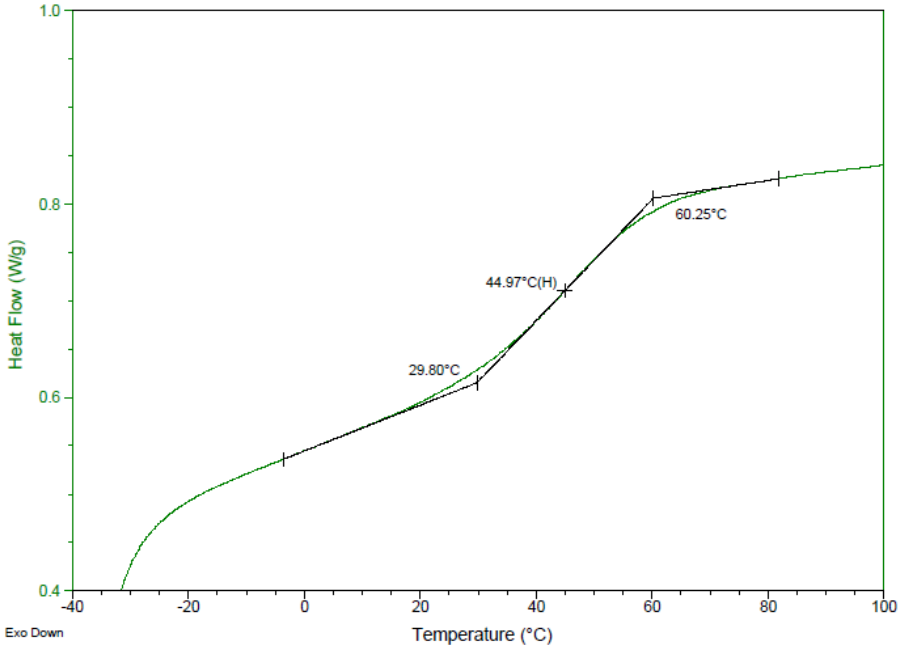

Figure 40 – DSC second cycle thermogram of specimen cured with cycle (1).

From Figure 40 it is possible to observe a T_g value of 45°C, which is comparable to the one obtained in the first cycle; this means that curing in the oven at 50°C for 3 hours

lead to the complete resin curing, as already hypothesized due to the lack of exothermic signals detected in the first heating cycle.

A necessary remark about this curing cycle is that resin, at the end of the cooling step, tends to remain partially *rubbery*, owing to the fact that the actual glass transition stems over a wide range of temperature, reaching almost Room temperature*;* so, in order to try to solve this aspect and to reach a value of T_g closer to the one declared by the producer, another curing cycle in the oven at higher temperature was tested.

Curing cycle (2):

- Start from room temperature (~30 min corresponding to mixing time);
- ramp of 0.5 °C/min until reaching a temperature of 70 °C;
- 3 hours at 70 °C;
- cooling inside the switched off oven.

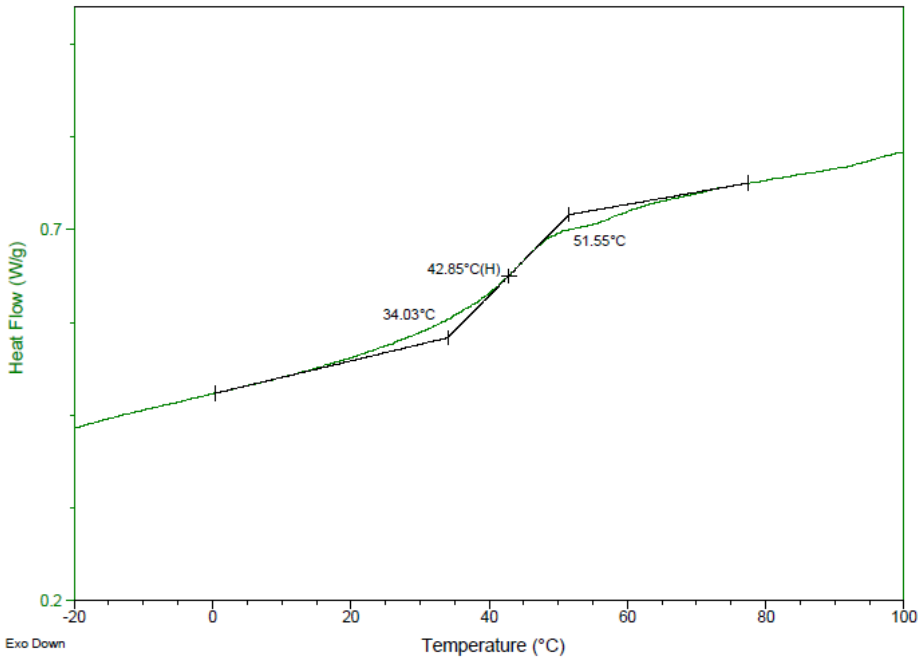

Figure 41 - DSC first cycle thermogram of specimen cured with cycle (2).

Observing the elaboration of the first cycle thermogram reported in Figure 41, the value of T_g remains lower than the one indicated by the manufacturer and comparable to the one observed in Figure 39. Once again, however, no sign of exotherms is recorded, suggesting that no significant reaction is promoted in the applied conditions.

Also in this case, the second DSC cycle is elaborated and reported in Figure 42.

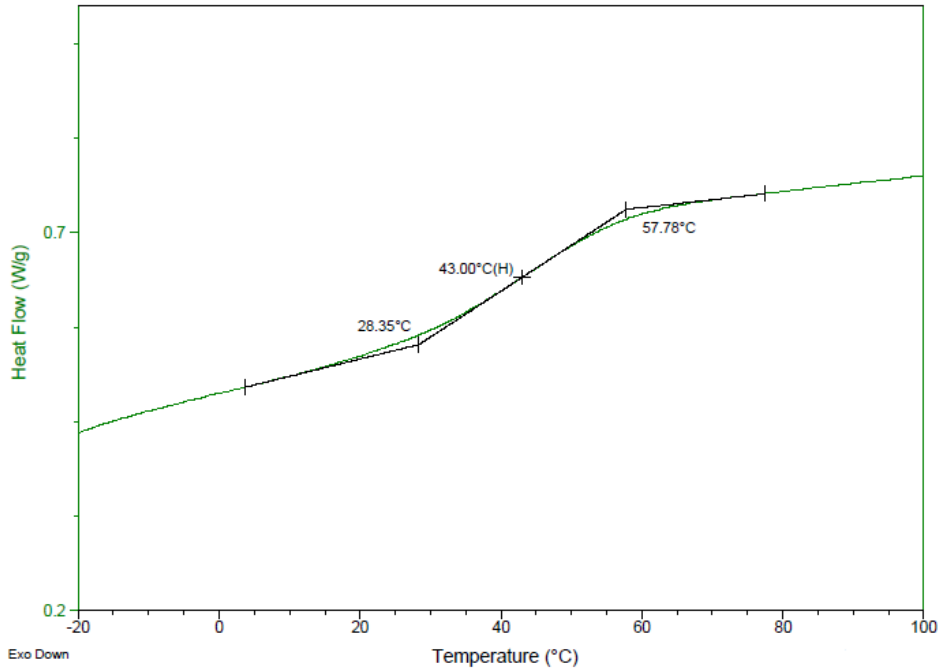

Figure 42 - DSC second cycle thermogram of specimen cured with cycle (2).

The T_g value obtained in the second cycle is the same of the first one, so also in this case curing of the resin was done in efficient way.

In conclusion, reaching a higher temperature during the curing process doesn't make T_g change in a significant way, given that both results are comparable between them and with the value reported in the datasheet.

So, given that there are no significant differences between the two curing cycles and that no additional analyses have been made, the selected curing cycle is (B): T_a → 70°C (0.5°C/min) + 3h 70°C.

<u>Uncured specimens</u>

For what concerns uncured specimens, two different curing cycles were tried using DSC. The aim of this is to simulate the curing cycle that occurs in the oven and to evaluate what is the maximum reachable T_g value using the two curing cycles reported in Table 1.

Method A	Method B
1: Equilibrate at 40.00°C	1: Equilibrate at 40.00°C
2: Data storage: On	2: Data storage: On
3: Ramp 0.50°C/min to 50.00°C	3: Ramp 0.50°C/min to 70.00°C
4: Mark end of cycle 1	4: Mark end of cycle 1
5: Isothermal for 180.00 min	5: Isothermal for 180.00 min
6: Mark end of cycle 2	6: Mark end of cycle 2
7: Ramp 10.00°C/min to -20.00°C	7: Ramp 10.00°C/min to -20.00°C
8: Mark end of cycle 3	8: Mark end of cycle 3
9: Ramp 20.00°C/min to 120.00°C	9: Ramp 20.00°C/min to 120.00°C
10: End of method	10: End of method

Table 1 - Two different methods log used for DSC analyses of uncured resin.

In Figure 43 and Figure 44 are reported DSC thermograms related to curing Method A and Method B respectively.

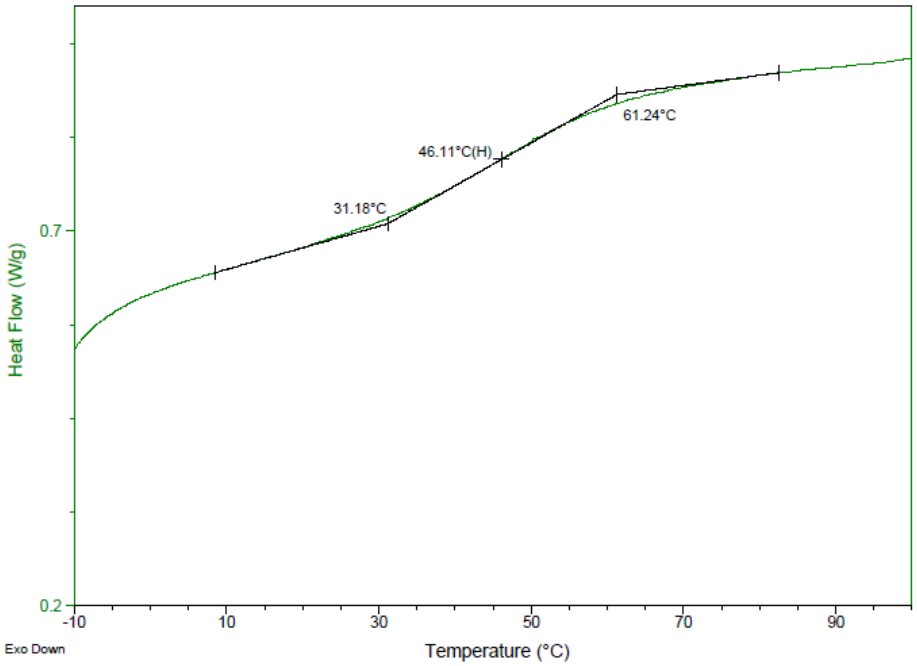

Figure 43 - DSC thermogram of resin cured with method A.

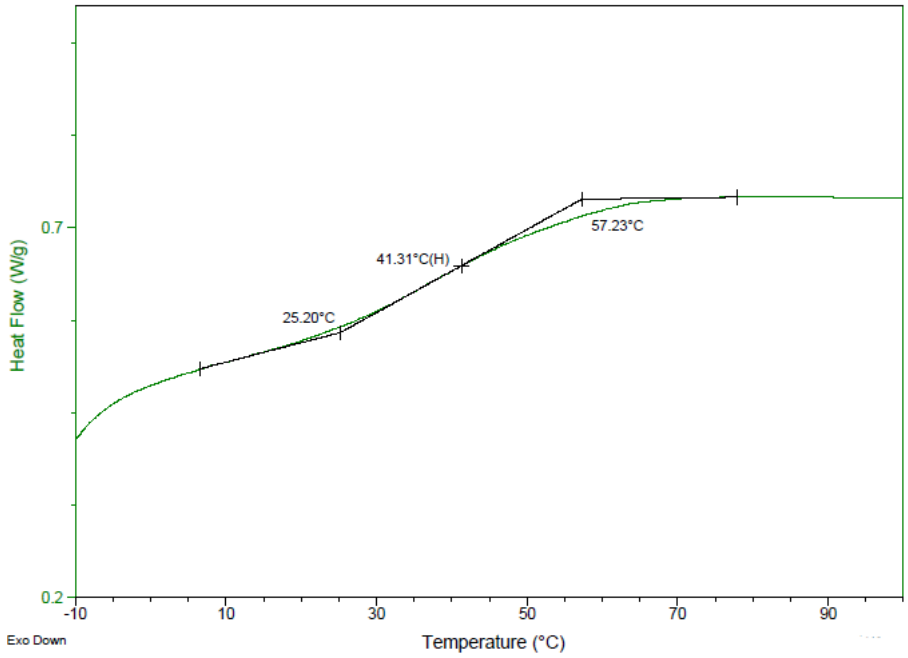

Figure 44 - DSC thermogram of resin cured with method B.

Method	**T_g [°C]**
A	46
B	41

Table 2 – DSC results for curing Method A and Curing Method B.

Analysing DSC results for uncured resin demonstrates that a T_g of 46 °C is obtained with 3 hours curing at 50 °C, while a T_g of 41 °C is obtained with 3 hours curing at 70 °C (in both case the ramp was 0.5 °C/min). The latter results is probably stemming from a too fast reaction, that lock macromolecular chains in an unoptimized condition, preventing a higher interconnection of the chains and a tighter network, eventually resulting in a higher T_g. However, no significantly higher T_g is attained and this confirms that there are no appreciable differences between the two curing cycles; in addition, results are comparable also with those observed for bulk cured resin and thus with producer datasheet.

All these considerations confirm that the choice to cure in the oven at 70 °C for 3 hours is right.

.

3.2 Adherends surface preparation

In the following sections, results regarding abrasion (Paragraph 3.2.1), chemical etching (Paragraph 3.2.2 and contact angle tests made on treated aluminium (Paragraph 3.2.3 are exposed.

This step is fundamental and must be carried out with extreme attention in order to produce an optimal surface for bonding. Mechanical treatments are done before chemical etching.

3.2.1 Abrasion

Abrasion is performed following the instructions given in the paragraph 5.2.1. Abrasion helps to remove machining scratches; this is important because otherwise, chemical etching would generate preferential roughness on the scratches and in addition the roughness wouldn't be homogeneous all over the surface.

The optimized abrading method is reported in Table 3.

Abrasive disc grit	Time (min)	Speed	Pressure (bar)
200	Until machining marks removal	Medium (5 on a max of 10)	1.4
400	2	Medium (5 on a max of 10)	1.4
800	2	Medium (5 on a max of 10)	1.6
1000	3	Medium (5 on a max of 10)	1.8
2500	5	Medium (5 on a max of 10)	2

Table 3 – Optimized abrading method.

Sandpaper disks of increasing grit are used in order to better remove machining scratches and marks of rougher sandpaper. After this step, adherents are washed with tap water, dried in order to avoid the formation of oxide only in certain zones, and lastly washed with acetone to remove possible impurities.

3.2.2 Chemical etching

After an accurate literature review regarding surface treatments for aluminium ([35]–[37], [43]–[45]) the optimized method reported below has been identified as the best (it includes also the first step of mechanical abrasion). A remark that has to be done is

that the P2 etch solution used is always half new and half recycled from previous treatments because this last is already activated by the presence of a certain quantity of aluminium, as reported in the references cited above.

1) Abrasion using automatic lapping machine;
2) Washing with tap water, drying, rinsing with acetone;
3) Rinsing with isopropyl alcohol;
4) Pickling: immersion in a glass Beaker containing the solution of NaOH (100g/L), at a temperature of 60°C for 1 minute: an inox steel support is produced and put inside the Beaker in order to hold up the adherends and to allow the solution stirring with a magnetic rod.

   In this step, a copious quantity of bubbles is formed, following the reaction reported in Section 1.7 .
5) Fast immersion in a plastic container with sacrificial tap water (this phase must be performed very quickly in order to avoid contact with air and it is fundamental to prevent contamination of immersion water);
6) Immersion in a plastic Beaker containing tap water for 10 minutes; at the same time sonication until complete cleaning of the surface must be made. Indeed, a gelatinous layer of impurities is formed during pickling because corrosion of aluminium occurs;
7) Drying with paper; avoiding rubbing;
8) Rinsing with isopropyl alcohol and waiting until it is completely evaporated from the aluminium surface;
9) Immersion in P2 etching solution (half new, half recycled from previous treatments) at a temperature of 65°C for 12 minutes (the configuration is the same of NaOH solution: inox steel support and magnetic rod).

   The solution must be previously activated with a piece of aluminium for 10 – 15 minutes, depending on the quantity of recycled solution used;
10) Repeat point 5);
11) Repeat point 7): also etching causes the formation of impurities that must be eliminated with sonication;
12) Drying with paper, avoiding rubbing;
13) Cleaning with isopropyl alcohol (also in this step, rubbing must be avoided in order to avoid scratches on the treated surface);

14) Leaving the aluminium adherend in contact with air for 3-4 hours to allow the formation of a new oxide layer.

Figure 45 shows the surface morphology of the aluminium adherends treated with the complete chemical etching process.

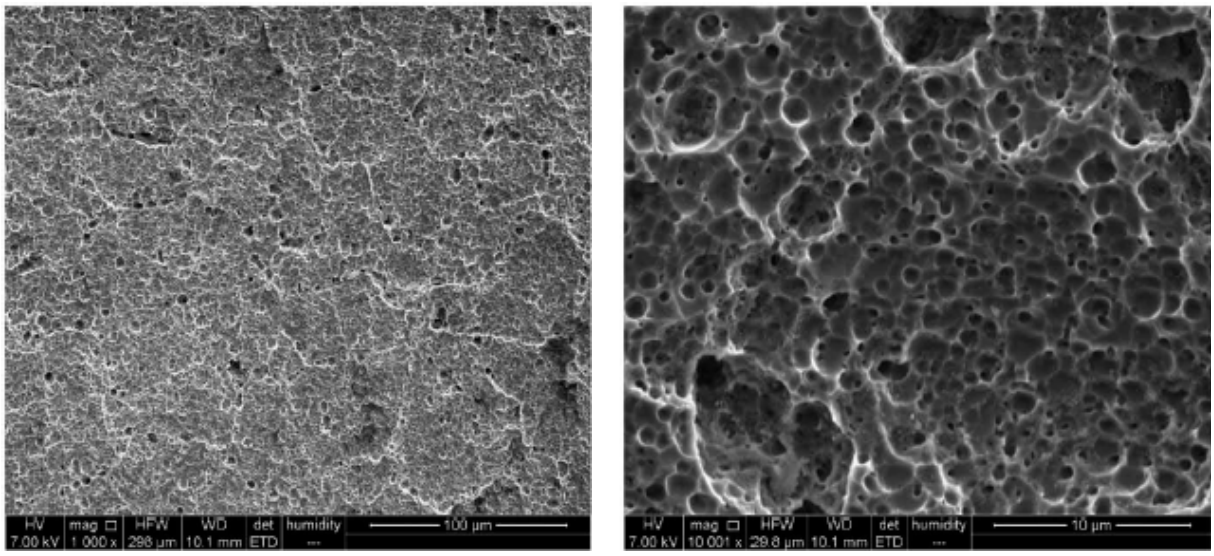

a) b)

Figure 45 – SEM image of aluminium adherends surface morphology after preparation at 1000x (a) and 10000x (b) magnification.

3.2.3 Contact angle tests

For what concerns the type of surface treatments analysed, four different batches are considered: only abraded (1), only pickled with NaOH (2), only etched with P2 solution (3), complete etching treatment (NaOH + P2 solution).

This test was performed using water instead of resin because with the available instrument there was no possibility to use resin; so, the aim of these tests was to obtain comparative results and not absolute values of contact angle.

In Figure 46 below wettability results are reported to allow the comparison of the different surface treatments. The position on the ordinate suggests the mean of the contact angle measures, while the diameter of the circles is a representation of the standard deviation: the bigger is the diameter, the higher is the standard deviation value.

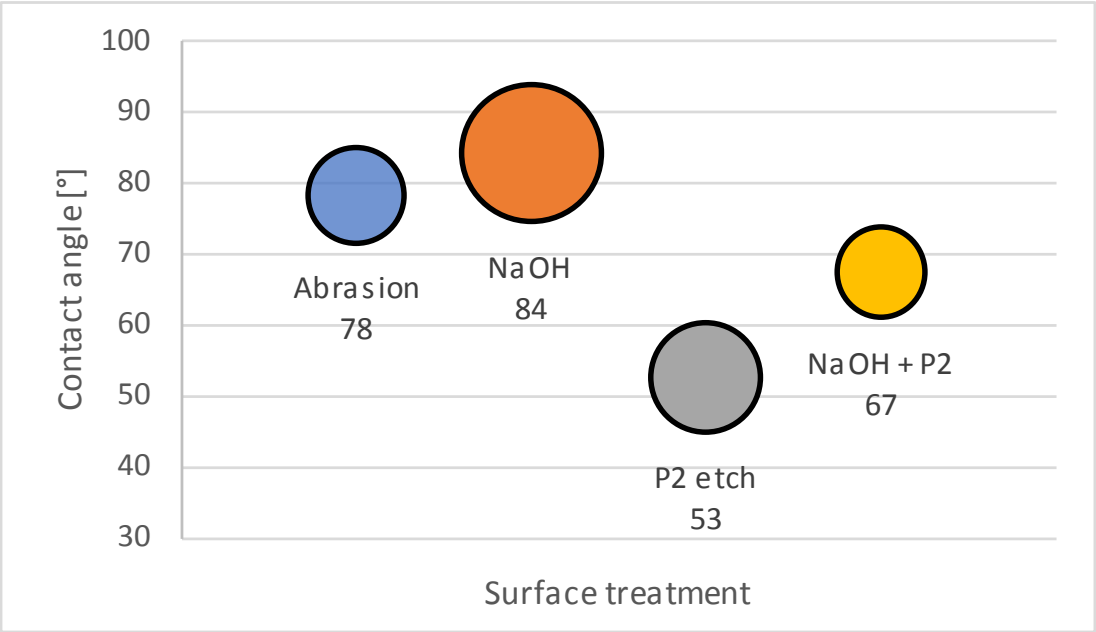

Figure 46 – Contact angle test results after four different surface treatments: abrasion, NaOH, P2 etch and NaOH + P2 etch.

It is clear that an optimum treatment cannot be identified with precision from this test. We expected the treatment (4) would have been the best one in terms of wettability, in particular after an accurate literature review.

Even if the combination of NaOH pickling and P2 etch seems not to be the most appropriate treatment, the step with NaOH can't be skipped: its function is indeed fundamental to degrease aluminium surface and perfectly remove impurities and machining lubricants.

3.3 Nanomat-Prepreg preparation and Thickness measurements

A Nylon nanomat has been prepared: its thickness varies between 50 to 95 μm, that however includes a high fraction of voids (even up to 85/90% v/v), while nanofibers that it is made of have a diameter of 480-500 nm, as later evaluated form Figure 47. After that, the nanomat is cut and then impregnated with resin. In previous works by Musiari et al. [46], this step was made using a spatula to remove resin excess: this led to unsatisfying results firstly because the nanomat seemed to be floating in the resin and then because the friction action of the spatula on the nanofibers tend to stretch and deform them. In the present work instead, the use of two counter-rotating drums, as explained in Section 5.4, allowed the removal of the excess of resin: the impregnated nanomat is put between them and resin is gently squeezed away in the

lateral part of the drums; in this way no deformation occurs and the quantity of resin results calibrated.

After this step, joining and curing occur as described in Section 5.4 and the thickness of the nanomat is measured.

Regarding cured specimens, the thickness of the nanomat is evaluated as reported in Section 5.4.2. A 50 μm thick EM252 nanomat is analysed with SEM after impregnation, bonding and curing.

To better appreciate the presence of nanofibre all over the adhesive thickness, three different treatments were tried.

1) Rubbing with paper drenched with formic acid.

   The dissolving action of formic acid towards nylon nanofibers is clear as reported in Figure 47 (b); contemporary the rubbing action helps mechanical removal of the solubilized polymer, at least in the outermost layers so it is easy to appreciate the presence of nanofibers all over the adhesive thickness, observing the nanometric holes left behind upon thermoplastic removal. For imaging purposes, indeed, it is not required a deep removal of the nylon component, but just enough to appreciate the moulded hole left empty.

   The SEM image (Figure 47 (a)) post-analysis reports an adhesive thickness of 50.3 μm, which is the same of the dry nanomat.

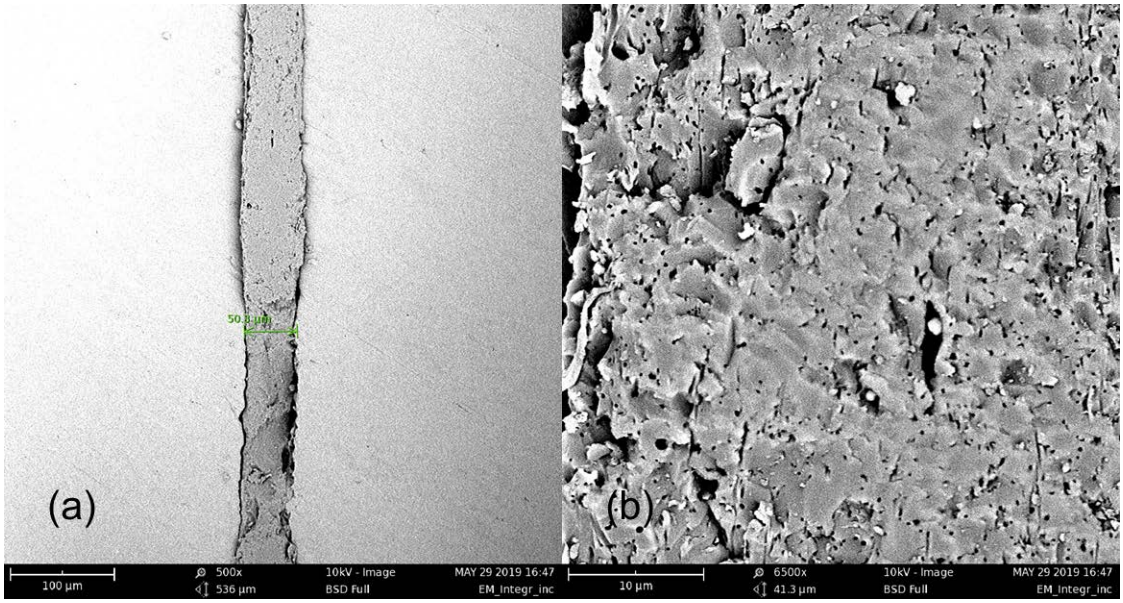

Figure 47 – (a) Thickness of the nano-reinforced adhesive and (b) Adhesive surface after Rubbing with paper drenched with formic acid.

2) Cleaning with acetone.
   Action of acetone on nanofibers is not strong enough to allow their dissolution so they are not well visible in the adhesive.

3) Specimen left immersed in formic acid for 1 hour.
   Dissolving action of formic acid is too strong; it also acts on epoxy adhesive producing void sections as it is shown in Figure 48.

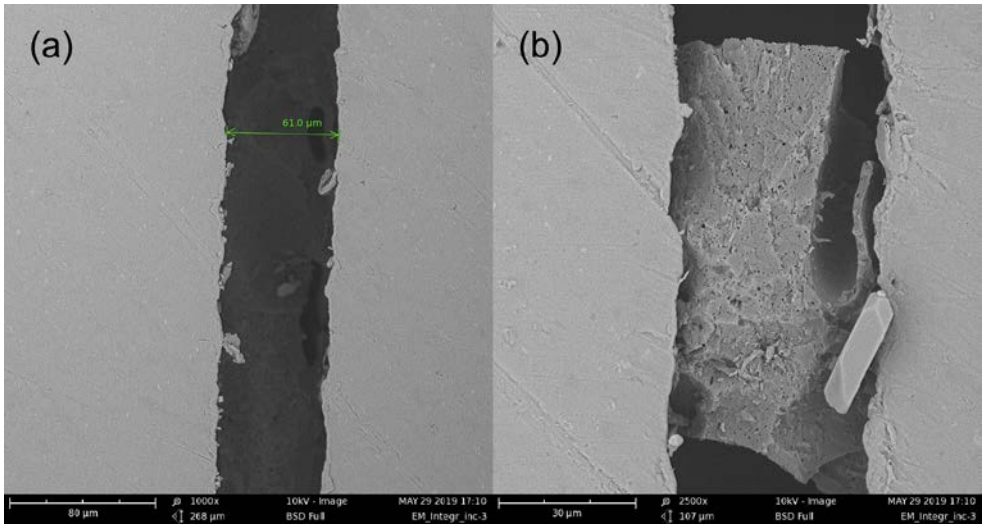

Figure 48 – (a) Thickness of the nano-reinforced adhesive and (b) adhesive surface after immersion in formic acid for 1 hour; it is clear the presence of resin voids.

The SEM image post-analysis reports an adhesive thickness of 61.0 µm, which is a bit higher than the one of the dry nanomat.
Anyway, considering the results in test 1) and 3), it is possible to say that no/little excess of resin is present in the impregnated nanomat; so, resin pockets, which would represent zones of preferential and easier crack propagation, are safely ruled out.
Thus, a successful result is the production for the first time in literature of a Nylon nanofibers prepreg.

In addition to thickness measures, the diameters of the holes left by the dissolved nanofibers are evaluated in order to check if they underwent compression or in general some kind of modifications; reference values are reported in Paragraph 5.3.2. After elaboration, the mean of the diameters results to be 480 nm while the standard deviation is 80 nm; these results are comparable to the reference ones, so nanofibers did not face any type of compression or dissolution.

3.4 DCB test results

In this section, DCB results are analysed and discussed.

In the first battery of tests, 3 virgin (V) specimens and 9 EM252 nano-reinforced (N) specimens are tested. Final fracture toughness, maximum applied load and crack length are obtained.

Force-displacement and fracture toughness-crack length curves are obtained with the recorded data for virgin and the nano-reinforced specimens and they are compared to understand the effect of the nanofibers on the bonding.

3.4.1 Virgin specimens

The first specimens tested are the virgin ones, in order to obtain baseline values of maximum force resistance to compare to the nano-reinforced ones.

As reported in Figure 49, the peak load of 105N was reached when the displacement of the crack arrived at approximately 1mm. After this point, curves are characterized by the typical loading-unloading trend (jump and arrest); peaks correspond to the maximum load that the adhesive is able to sustain at the indicated crack growth. Every time there is a loss of load, the crack starts to propagate; at each minimum of the curve, the crack stops propagating, and it resists until the following peak, where load is too high and leads to another loss of force.

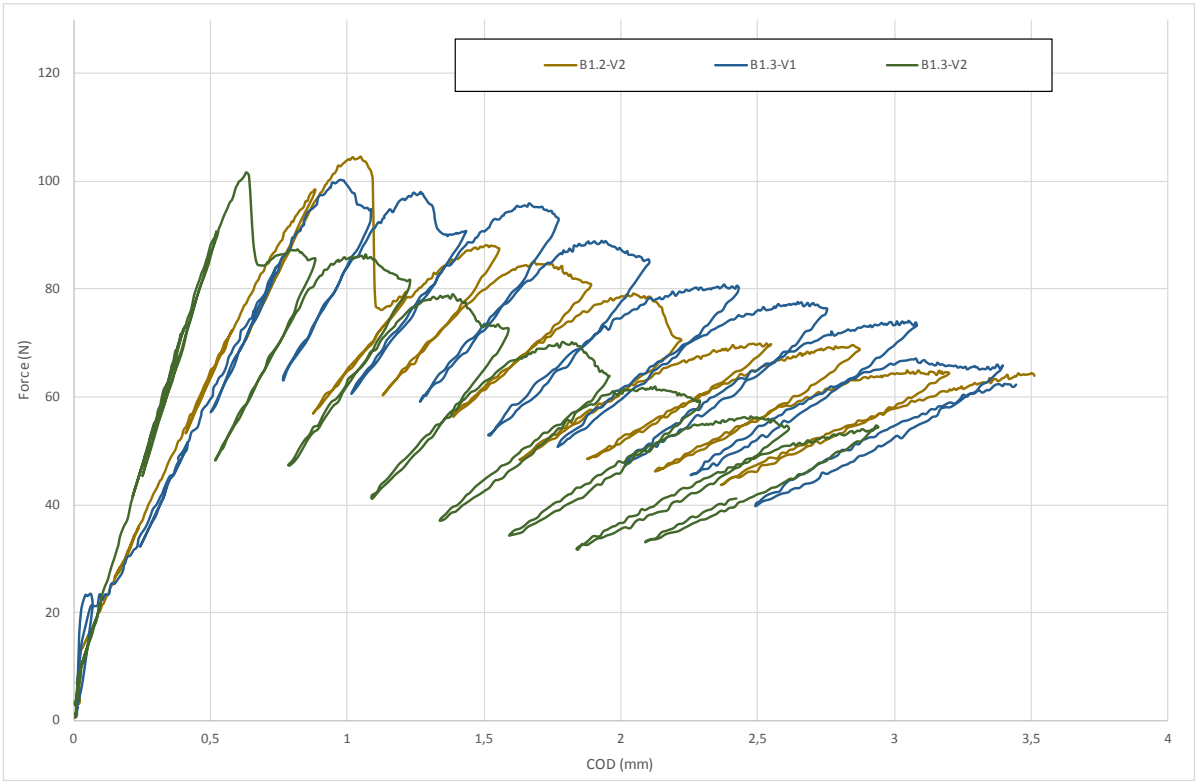

Figure 49 – Force vs. CMOD curve for virgin specimens.

After DCB test, bonding surfaces are analysed in order to understand if fracture occurred in adhesive or cohesive way.

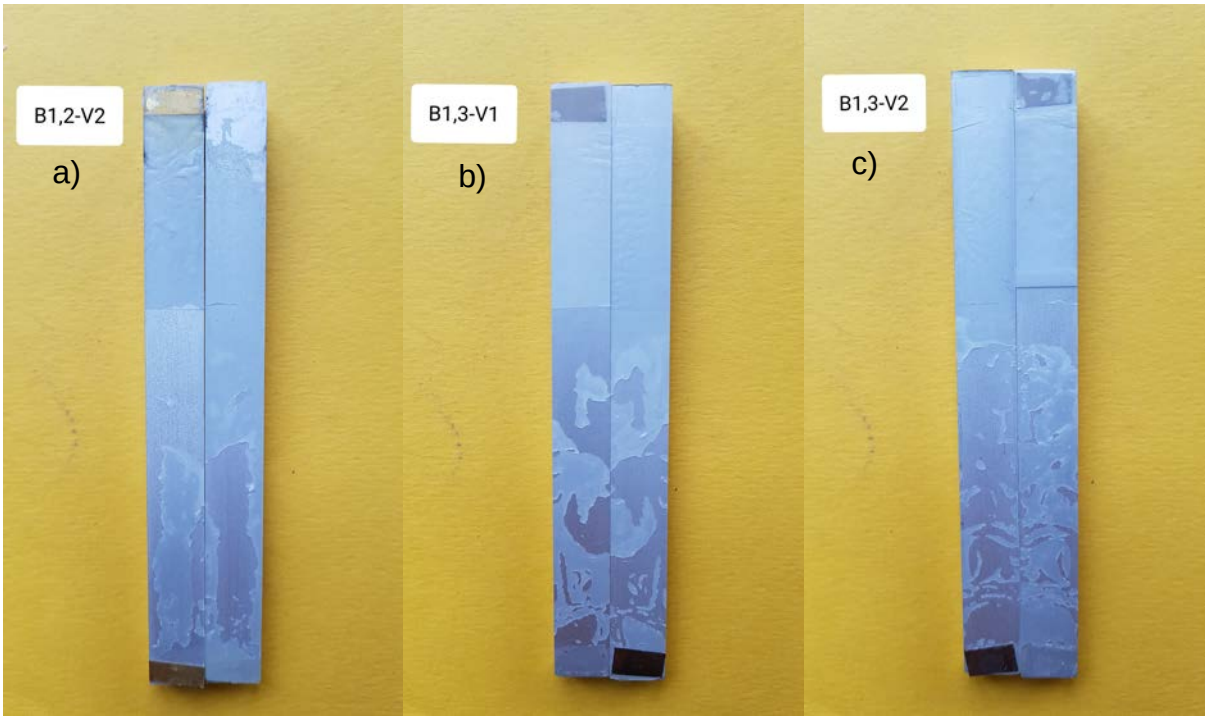

Figure 50 – Fracture surfaces of virgin specimens.

After observing Figure 50, different considerations can be made.

- Specimen B1.2-V2: the fracture is completely adhesive. Indeed, in the first part the crack proceeds on the surface on one adherend, then with a mechanism of crack deflection, it passes on the other adherend.
- Specimen B1.3-V1: also in this case fracture is completely adhesive, but here the cracks is deflected form an adherend to the other a higher number of times with respect to the first specimen.
- Specimen B1.3-V2: the crack propagated mostly on the interface of only one of the two adherends (the left one); it can be said because the majority of the adhesive is present only on one adherend (the right one).

After fracture occurs, one of the specimens was analysed with SEM and micrographs were taken.

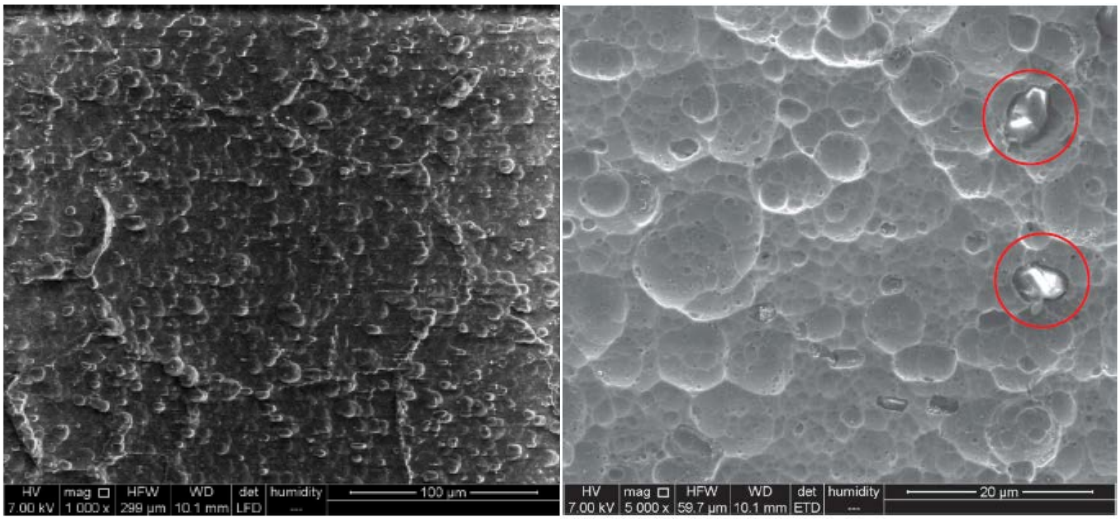

(a) (b)

Figure 51 - SEM image of the fracture surface of a V specimen (adhesive side) at 1000x (a) and SEM image of the same specimen with magnification 5000x showing a few adhesive leftovers entrapped in surface pits (circled in red).

The surface is quite pickled thanks to P2 etch, but as it is possible to see in Figure 51 (b), anchor points, where the adhesive remained joined to the surface, were very limited in number. Probably, manufacturing conditions, that include the use of copper spacers as a way to guarantee the same thickness of the nano-reinforced joints, lead to a non-uniform application of the load applied while curing and thus may not yield to the same pressure as in the case of N joints, where there are no spacers.

Since keeping the same adhesive layer thickness is absolutely essential in order to have a reliable comparison between N and V joints, an even more effective surface preparation has to be developed in order to ensure enough adhesion in all cases.

3.4.2 Nano-reinforced specimens

Nano-reinforced specimens had different fracture behaviours so they will be divided in three group in order to better analyse and understand dissimilarities.

1) The first group includes three specimens (N-EM2.1, N-EM2.2 and N-EM2.3). All these specimens have a peak force higher than virgin ones, as shown in Figure 52, so a higher fracture toughness can be foreseen.

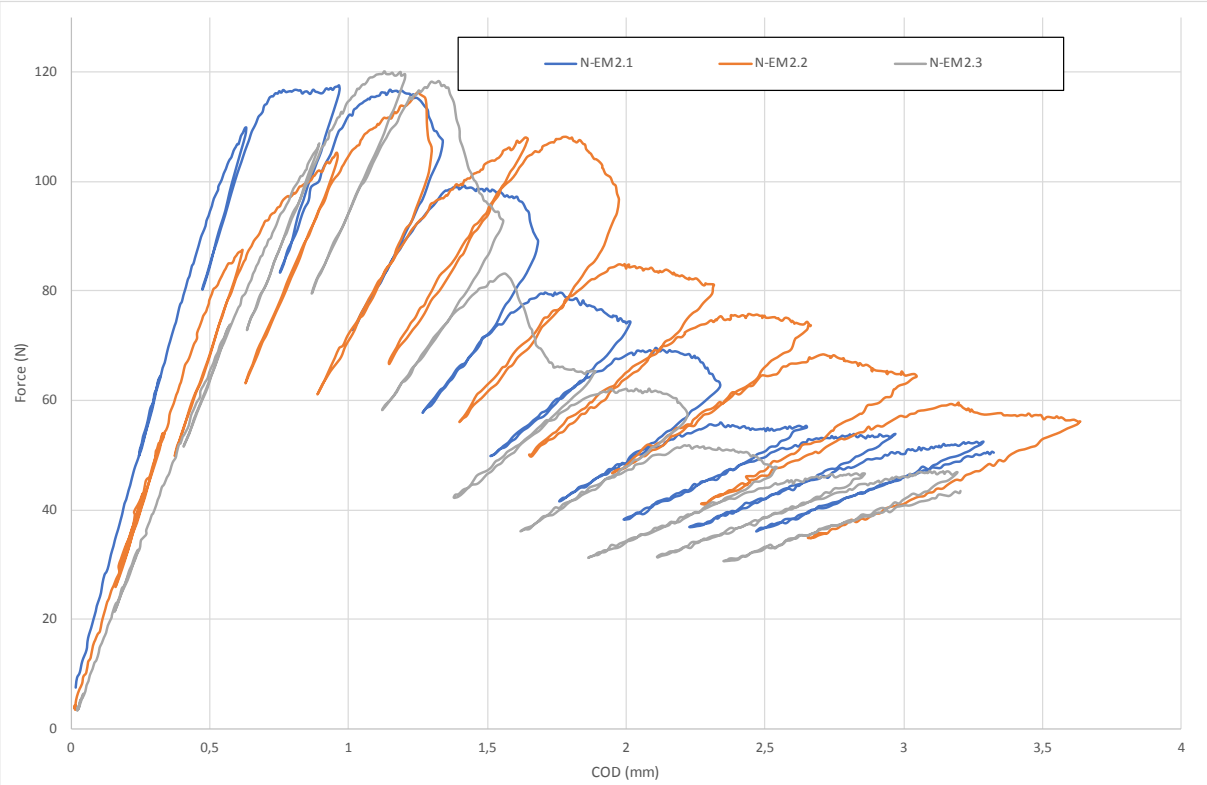

Figure 52 - Force vs. CMOD curve for nanomodified specimens (1).

For values of CMOD greater than 2 mm the overall trends of the nanomodified and virgin joints get closer, hence the force shows a sharper decrease in the case of N joints [42].

Therefore, in order to see if a difference in terms of fracture toughness persists, the whole R-curve, presented in Figure 53 is examined.

There is a major difference from what the analysis of the overall Force-CMOD data indicates: the N joints that start from values of G_c comparable or lower than the V ones (average value 0.23 N/mm against 0.26 N/mm) may imply a similar crack initiation mechanism.

Indeed, with increasing crack propagation (4-8 mm), the fracture toughness of N joints increases more rapidly than that of V joints; that means that some kind of toughening mechanism related to the nanofibers develops. This is supported, for crack propagations in the range reported above, by the fact that the scatterbands of N and V joints, represented in Figure 53 by the average value ± one-half standard deviation, are not overlapped.

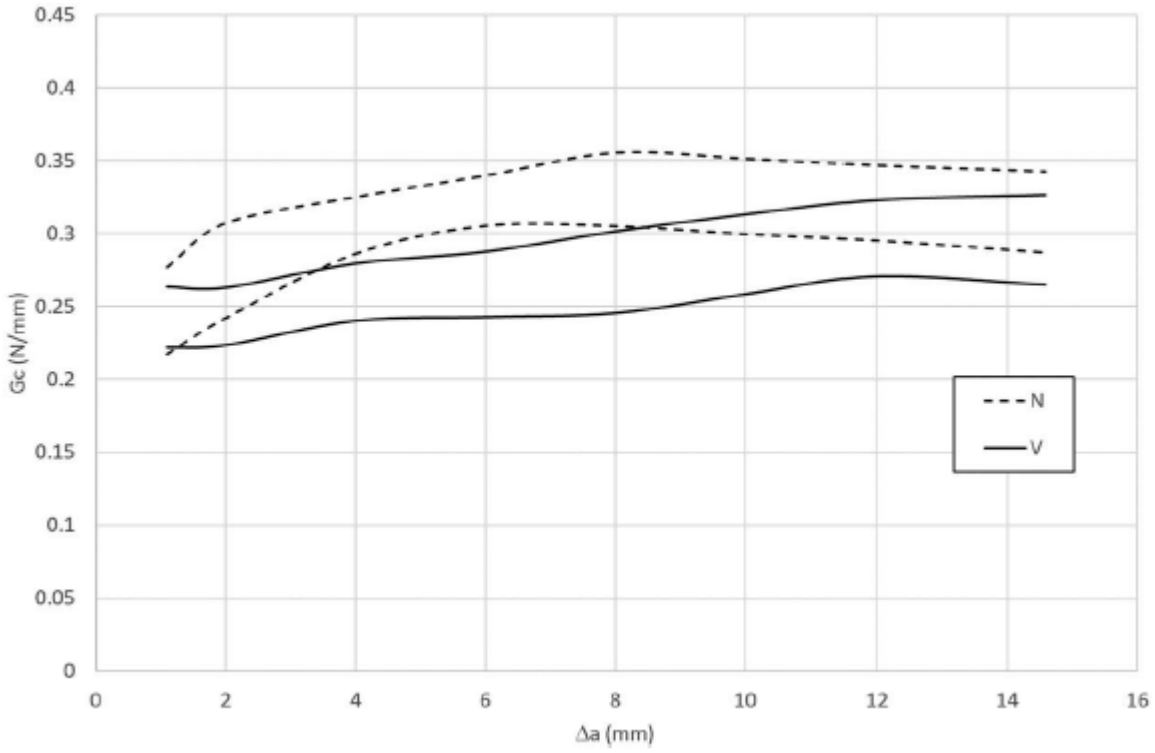

Figure 53 - Fracture toughness vs. crack propagation. The lines represent the scatterband of experiments (average value ± one-half standard deviation).

From the visual inspection of Figure 54, that shows the fracture surfaces of the three nano-reinforced specimens, it is impossible to distinguish a different failure mechanism in comparison to the virgin ones, shown in Figure 50; the failure is at or close to the interface despite the etching treatment of the aluminium adherents and the low thickness of the bond line. This mechanism of crack propagation may justify also the relatively moderate value of fracture toughness for a structural adhesive.

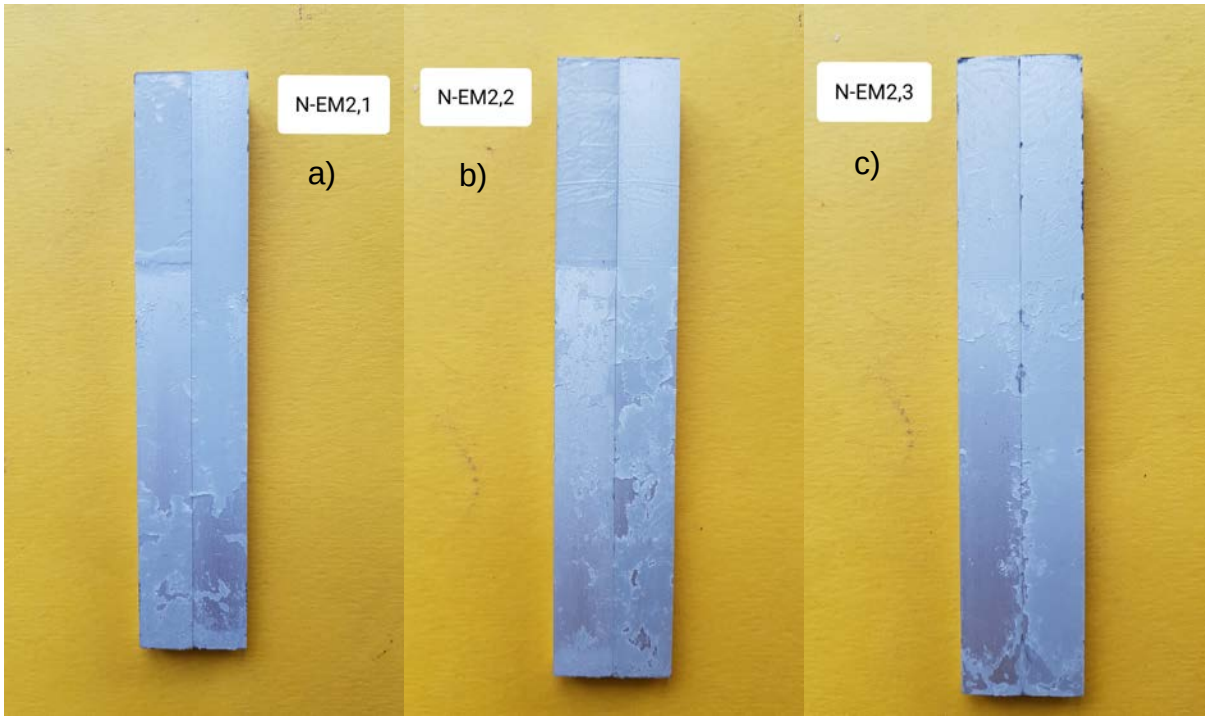

Figure 54 – Fracture surfaces of nanomodified specimens (1).

Fracture surfaces are characterized by frequent crack path deviations from close to one adherent to the other one, but in Figure 54 some adhesive seems to be left also on the brighter side, that may justify the higher fracture toughness with respect to virgin specimens.

In the case of c), the crack path deviations were less frequent; therefore, the value of G_c, initially higher than V joints, decreased with crack propagation approaching the one of the virgin c) joint, where a similar crack path was detected. So, the joints that performed better seems to be those with more frequent crack path deviations: the cause of that may be a higher quantity of energy dissipation involved in crack deviation.

In order to understand if N joints do have some residue of adhesive on the brighter adherent and then why they perform a little bit better than V joints, the fracture surfaces were examined at the SEM.

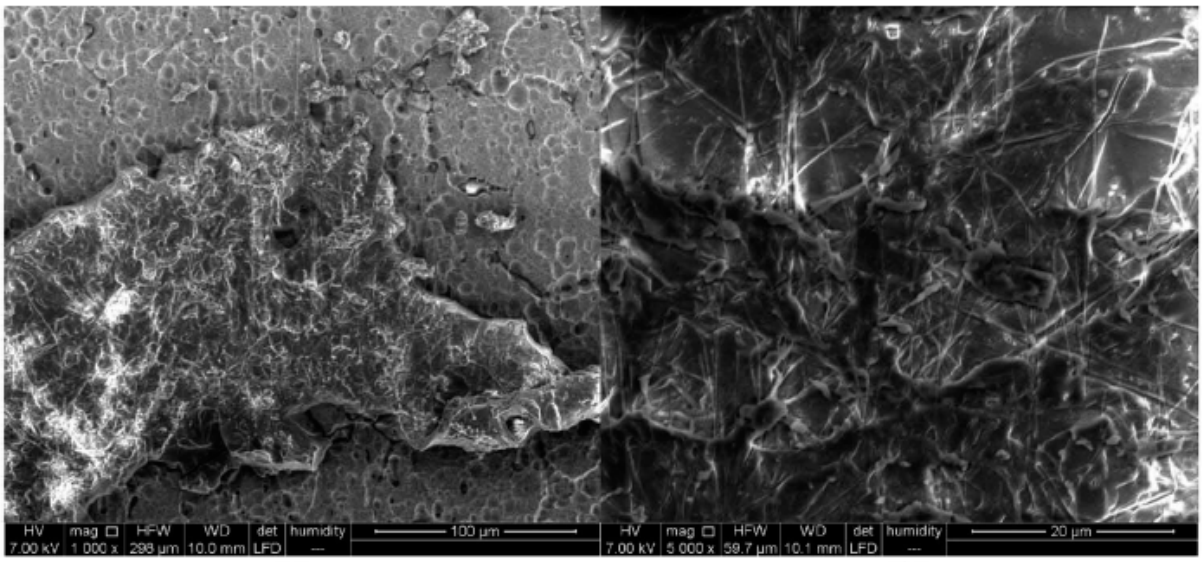

(a) (b)

Figure 55 – SEM image of the fracture surface of a N specimen at 1000x (a) and 5000x (b) [42].

In Figure 55 the crack did not progress into the nanomat (in fact it is possible to see the pickled aspect of the naked aluminium surface due to P2 etching) but ripples of adhesive+nanomat are left in correspondence of deeper grooves on the surface that act as anchor points.

Observing Figure 55 (b), which reports the same zone of Figure 55 (a) but with a higher magnification, it is easy to see the presence of nanofibers in the adhesive but without signs of fibre pull-out due to crack bridging.

In conclusion, it seems that the presence of a relative high number of anchor points is enough to guarantee a fracture toughness comparable or tendentially higher than that of the virgin specimens, where anchor points were many less in number.

2) The second group of nano-reinforced specimens includes only one of them (N-EM2.5A). This specimen has a load peak of 105 N, that is almost the same value of virgin joints. Observing the graph in Figure 56, is possible to appreciate that also the trend of loss of load is very similar to the one of virgin specimens reported in Figure 49. Fracture occurs at approximately 3mm of CMOD value, which corresponds to the value obtained with the worst of the virgin specimens.

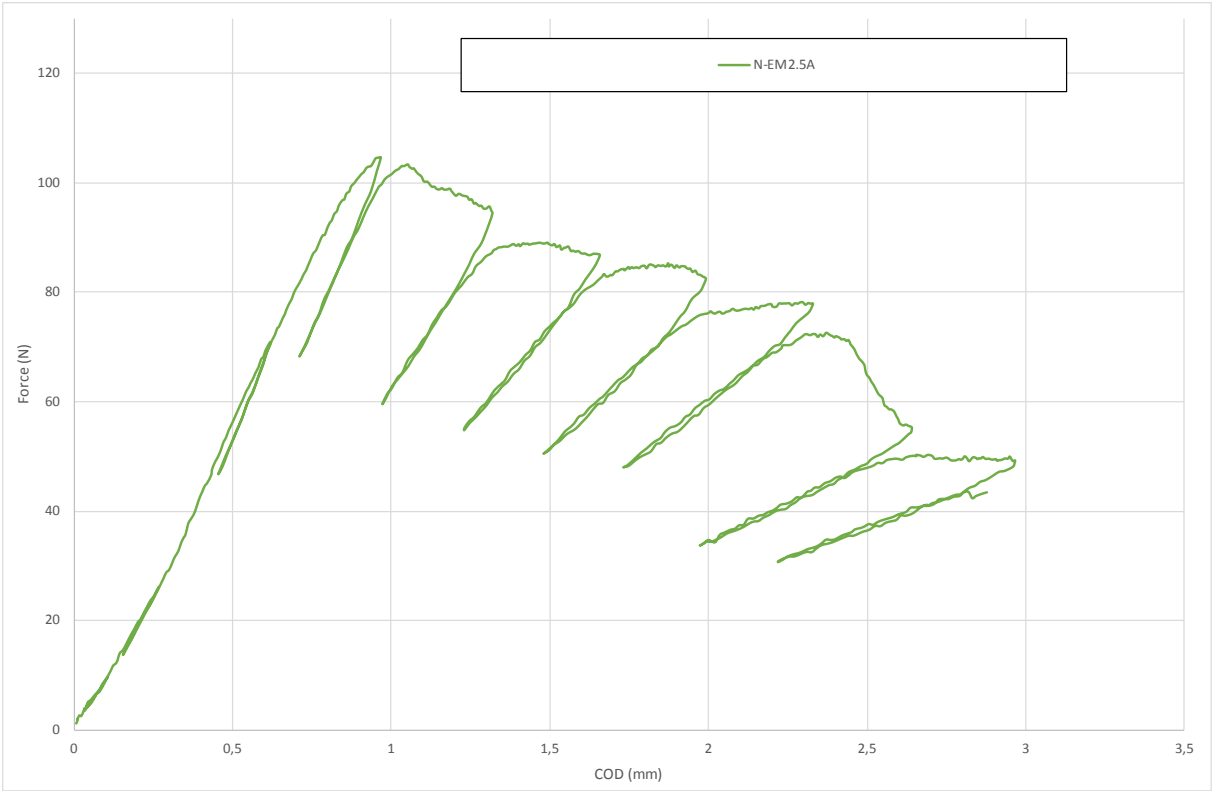

Figure 56 - Force vs. CMOD curve for nanomodified specimen (2).

From the visual inspection of the fracture surface reported in Figure 57, the first part after Teflon sheet corresponds to an adhesive fracture; at approximately half of the length of the adherend, fracture seems to occur through a cohesive mechanism (proven by the fact that on both surfaces adhesive is clearly visible).

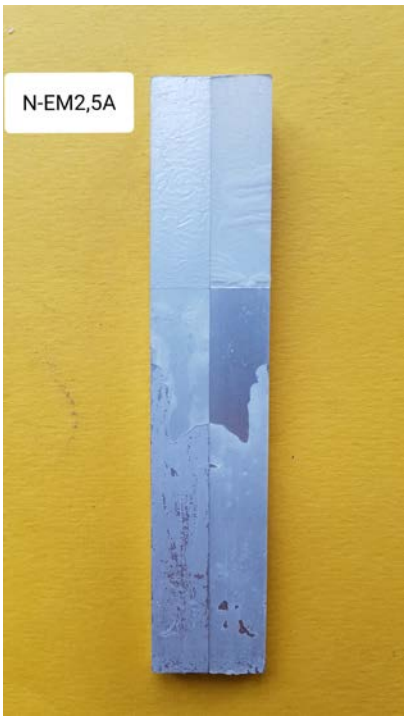

Figure 57 – Fracture surface of nanomodified specimen (2).

3) The third and last group of nano-reinforced specimens includes four joints (N-EM2.4A, N-EM2.4B, N-EM2.6A and N-EM2.6A). All these specimens have a peak force lower than virgin ones, as shown in Figure 58.

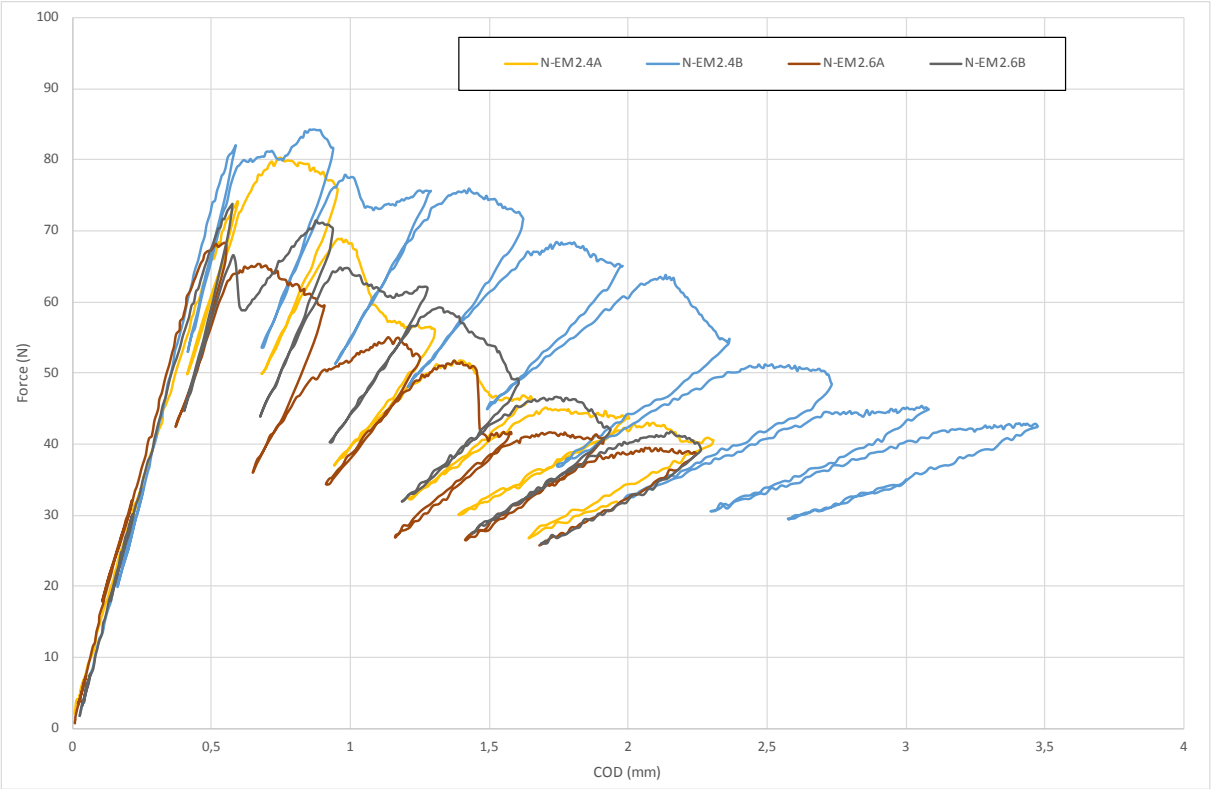

Figure 58 - Force vs. CMOD curve for nanomodified specimen (3).

In all cases except specimen N-EM2.4B, fracture occurs at values of CMOD not higher than 2.5 mm; this result is not satisfactory, given that those values are lower than the lowest of the virgin specimen, as it is possible to see in Figure 49. From the visual investigation of the fracture surfaces reported in Figure 59.

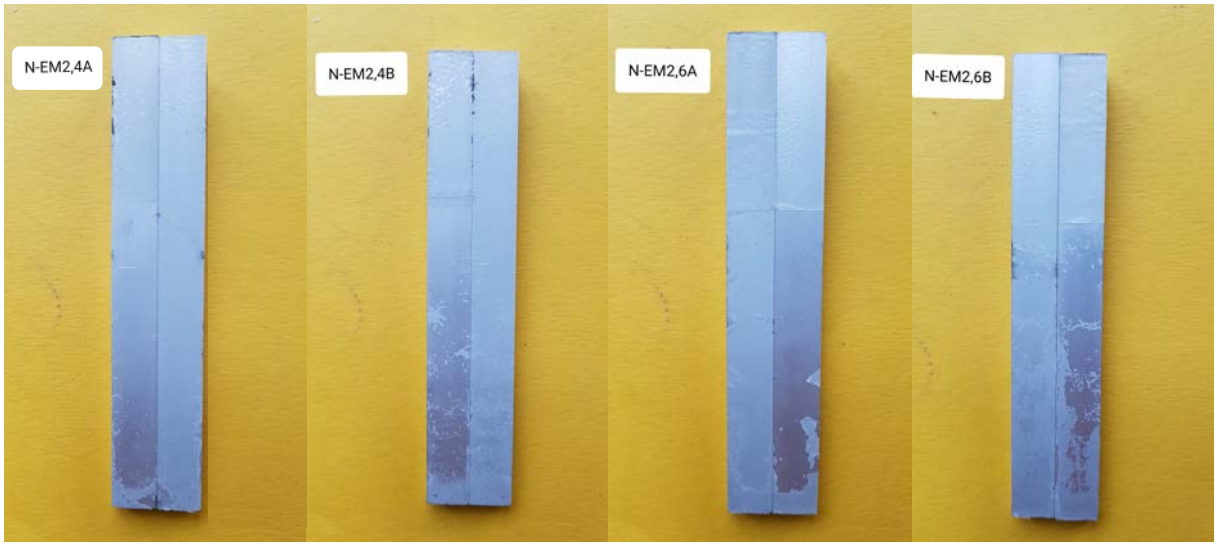

Figure 59 - Fracture surface of nanomodified specimen (3).

- Specimen N-EM2,4A: the fracture is completely adhesive. In the final part (~5mm), the fracture seems to be a mix between cohesive and adhesive;
- Specimen N-EM2,4B: also in this case fracture is completely adhesive, except is some zones in lateral part and at the end of the specimen, where a mixed cohesive and adhesive mechanism;
- Specimen N-EM2,6A: as the cases reported above, the crack mostly propagates on the interface of only one of the two adherends, so the fracture is completely adhesive, except the last 5mm;

Specimen N-EM2,6N: this specimen is the only of this group where a cohesive fracture occurs in an appreciable way; indeed, as it is possible to see in Figure 58, this joint is the best for this group, but not in absolute, in terms of load peak and crack propagation.

4. CONCLUSIONS

In the present work, the production of aluminium joints bonded with a nano-reinforced epoxy adhesive was developed in order to evaluate the enhancement of the mode I fracture toughness. Two different type of nanomat are produced, using two different solvent systems (EM252 and CB12); nanofibers are made of Nylon 6,6 and were obtained with electrospinning technique.

A first remarkable result is the production of a nanofibers prepreg; it was possible with the aid of two counter-rotating drums that calibrates the right resin quantity to impregnate the nanomat. This facilitates the application of the correct amount of adhesive at the surface. As concerns the actual adhesion of the aluminium samples, both virgin and nano-reinforced specimens were produced so that a comparison between the two was possible. Specimens were prepared with an optimized combination of mechanical and chemical surface treatments, cured with an optimized curing cycle and then tested with a Double Cantilever Beam test to evaluate a potential enhancement of fracture toughness in mode I of nano-reinforced specimens with regards to the neat ones. An improvement was observed in some cases, while in others the value of peak load was equal or lower to the one of neat specimens.

The effectiveness of fracture toughness enhancement using Nylon 6,6 nanofibers has been proved, even if only for three out of eight specimens. In most cases, fracture occurred in an adhesive way instead of cohesive, producing an interfacial fracture between the surface and the adhesive.

In subsequent studies specimens prepared with CB12 nanomat (which differs from EM252 for the solvent system that is formic acid (CH_2O_2) and chloroform ($CHCl_3$) in a ratio of 50:50 volume / volume) will be tested, in order to evaluate if they perform better than EM252. Moreover, given that the potential of the nano-reinforcement has been confirmed, the aim of following studies could be a more accurate control on the failure mode. Connected to this there is the surface pre-treatment, which should be studied deeply, in order to produce an even better bonding surface.

5. METHODOLOGY

In this chapter experimental procedure is described. In Section 5.1 resin features and DSC analyses method logs are reported. In Section 5.2 mechanical and chemical preparation of the adherends are exposed, while in Section 5.3 the production of nanofibrous mats is described. In Section 5.4 the whole production process of the joints is reported, while in Section 5.5 DCB tests are briefly described.

5.1 Epoxy adhesive

The epoxy resin selected for this work is the AS46 (hardener AW46), a bicomponent epoxy system provided by the company ELANTAS. It is a high viscosity system (38000 – 50000mPas) used for impregnation (it is not a structural resin, but the best of impregnation resins by this producer), necessary to impregnate nanofibers.

The company suggests a resin/hardener ratio of 100:80 w/w; it can be cured for 24 hours at room temperature, but the best curing cycle is 3h at 50°C, with which a T_g of 57-60°C should be reached (find with DSC test, technical data).

Because of its high viscosity, many tests were performed in order to remove bubbles from the resin, as reported in paragraph 3.1.1.

5.1.1 DSC analyses

Calorimetric analyses are made using a DSC modulated instrument (TA Instruments Q2000) connected to an RCS cooling system. All the measures are carried in aluminium pan containing from 4 to 8 mg of resin.

Reference: aluminium pan.

Test are made both on cured and uncured resin.

DSC Analysis Method Log for cured resin is reported below:

1: Equilibrate at -40.00°C

2: Data storage: On

3: Ramp 20.00°C/min to 120.00°C

4: Mark end of cycle 1

5: Ramp 20.00°C/min to -40.00°C

6: Mark end of cycle 2

7: Ramp 20.00°C/min to 120.00°C

8: End of method

For what concerns uncured resin instead, two different curing cycles were used: the first is the one suggested by ELANTAS, the second was a slightly different one. Results and considerations on DSC tests are reported in paragraph 3.1.3.

5.2 Adherends preparation

A 6082-T4 aluminium plate is cut and machined in order to obtain 100(l)x10(b)x5(h) mm^3 adherends. In Figure 60 is reported an example of the specimens.

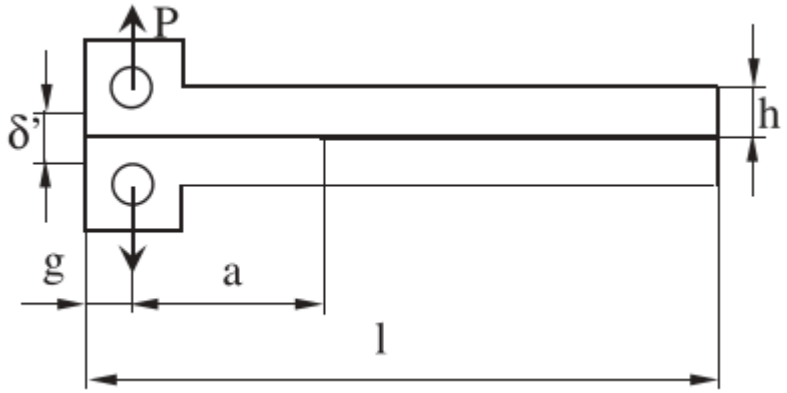

Figure 60 – Outline of the DCB test setup [42].

The dimensions of the specimens used in the present work are different from the standard ones, mainly for two reasons:

1) standard specimens would have been bigger and of different geometry: that means that a lot more material would have been necessary, making test more expensive;
2) these dimensions allow adherends to emphasize the mode I fracture behaviour of the resin;
3) results obtained are only comparative.

5.2.1 Abrasion

Abrasion is carried out with a lapping machine using a template that allows to automate the process. Sandpaper disks of increasing grit are used. The complete optimized process is described in paragraph 3.2.1.

5.3.1 Surface chemical treatments

Chemical surface treatment needs two types of solutions: a basic solution and an acid solution. The first one is necessary in order to degrease aluminium, while the second is fundamental to nano-structurate the surface and to form a surface suitable for adhesive bonding.

NaOH solution

The solution is prepared adding 100g of NaOH in pellets to 1L of distilled water.

The solution must be heated up to allow the reaction with aluminium (described in Section 1.7) and maintained in agitation with a heating stirrer in order to avoid the deposit of impurities on the aluminium surface.

P2 etching solution

1) Pour 50mL of water into a flask;
2) Add 75g of ferric sulphate $Fe_2(SO_4)_3$ 75% w/w;
3) Add 200mL of demineralized water;
4) Gently add 100mL of sulphuric acid H_2SO_4 97% (185g, d = 1.84 kg/L);
5) Slowly add enough demineralized water to reach 1L of total volume.

The optimized chemical etching method is reported in paragraph 3.2.2.

At the end of the surface preparation process, contact angle test were made using water as wetting liquid, in order to evaluate the wettability of the aluminium surface. The contact angle instrument is reported in Figure 61.

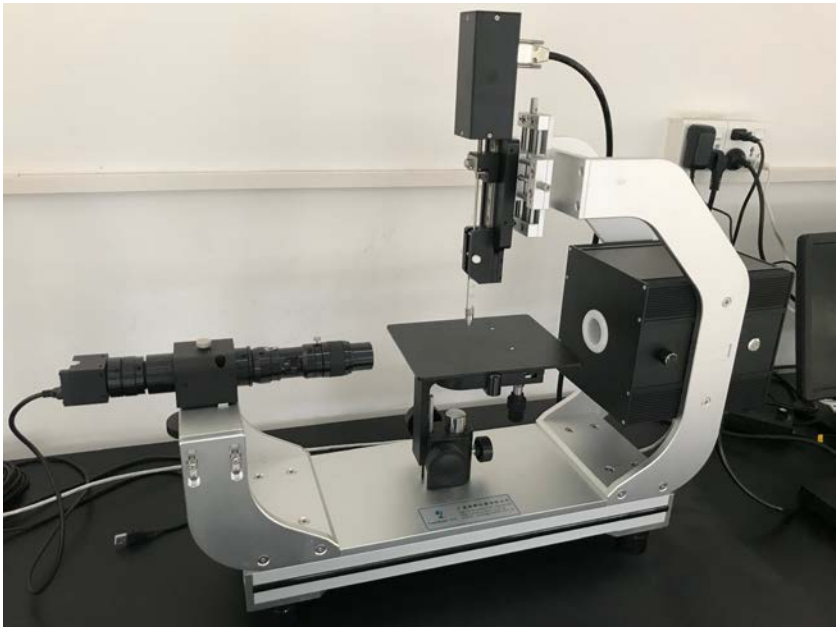

Figure 61 – Contact angle instrument.

Four different batches are selected: only abraded (1), only pickled with NaOH (2), only etched with P2 solution (3), complete etching treatment (NaOH + P2 solution) (4).

5.3 Polymeric nanofibrous mats (electrospinning process)

A polymeric solution is prepared using an appropriate solvent system.

The solution is prepared inside a vial; a magnetic rod is placed inside it after the mixture, which is stirred and heated (35-40°C) for 2-3 hours in order to facilitate polymer dissolution.

After that, the mixture is put inside a 5mL glass syringe; it is connected to the needle (ejection system) through a small rubber tube.

Once everything is settled, the process is started.

Two different solvent systems are used to produce Nylon 6,6 electrospun nanofibers, CB12 and EM252; specimens reinforced with CB12 nanomats have not been tested in the present work.

5.3.1 CB12 nanomat

This type of nanomat was obtained using Nylon 6,6 Zytel® E53 NC010 provided by DuPont, dissolved at a concentration of 14% solute weight / total solution weight (here in after w/v_{solv}) in a solution composed by Formic Acid (CH_2O_2) and Chloroform ($CHCl_3$)

in a ratio of 50:50 volume / volume (here in after v/v). The solution is prepared dissolving Nylon pellets in formic acid firstly and only later chloroform is added in order to lower viscosity and increase electrospinnability.
The electrospinning parameters to obtain these nanofibers were optimized by the Research Group on Electrospinning (RGE) team of the University of Bologna in a previous work [47].

Electrospinning parameters

Flow rate: 0.35mL/h

Voltage: 18.5kV

Distance (between the needle and the collector): 15cm

Relative humidity: 25 – 40%

Temperature: 24 – 26 °C

Electrospinning setup

Multi-needle configuration (two or four); needle diameter: 0.84mm. 5mL glass syringes are used. Rotating cylinder collector (50rpm) on which is placed a sheet of PE coated paper is used. Electrospinning setup is reported in Figure 62.

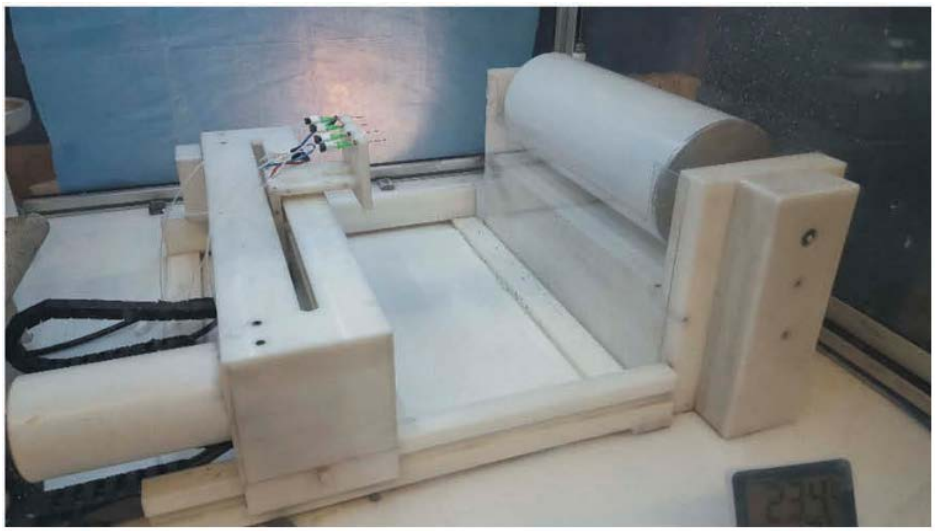

Figure 62 – Electrospinning setup with four needles configuration [42].

5.3.2 EM252 nanomat

This type of nanomat was obtained using Nylon 6,6 Zytel® E53 NC010 provided by DuPont, dissolved at a concentration of 13% w/v_{solv} in a solution composed by trifluoracetic acid (CF_3COOH), formic acid (CH_2O_2) and chloroform ($CHCl_3$) in a volume ratio of 10:60:30. The solution is prepared adding formic acid to trifluoracetic acid, dissolving then Nylon pellets and only later chloroform is added.

The electrospinning parameters to obtain these nanofibers were optimized by the Research Group on Electrospinning (RGE) team of the University of Bologna in a previous work [48] by E. Maccaferri.

Electrospinning parameters

Flow rate: 0.7mL/h

Voltage: 25kV

Distance (between the needle and the collector): 6.5cm

Relative humidity: 25 – 40%

Temperature: 24 – 26 °C

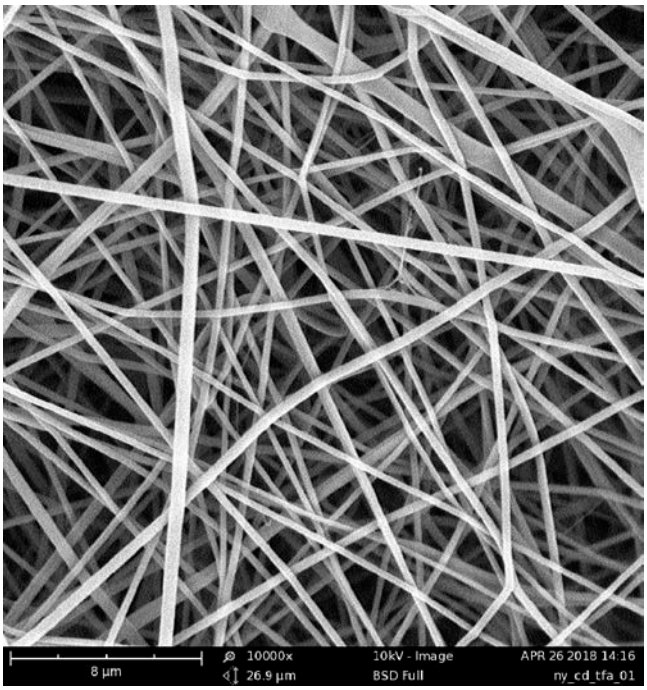

Figure 63 – Nanomat obtained with optimized electrospinning parameters.

In Figure 63 is reported the morphology of the nanomat that should be obtained with the electrospinning parameters cited above. After taking 25 nanofibers diameter measures, mean value is equal to 430 nm, with a standard deviation of 90 nm.

Electrospinning setup

Multi-needle configuration (two or four); needle diameter: 0.51mm. 5mL glass syringes are used. Rotating cylinder collector (50rpm) on which is placed a sheet of PE coated paper is used.

Cross reference to Figure 62 for what concerns four needles electrospinning setup. Before proceeding with specimen production, impregnation tests were made to evaluate if there are substantial differences for what concerns the resin wettability of the two nanomats.

The test is conducted following the steps reported below:

1) A small quantity of resin is poured in each section of a silicone template;
2) Small pieces of each nanomat are placed inside the template;
3) Resin is poured on the nanofibrous mat in order to impregnate it.

5.4 Production of the specimens

After the preparation of the adhesive as reported in 3.1.2 two different batches are produced.

Before specimen production, Teflon laminates and nanofibers mat must be cut, placed under vacuum for 10 minutes and in oven at 40°C for 2 hours.

Virgin batches (V)

For virgin specimens, copper laminates are placed in the adherend ends with the purpose of giving the resin the needed thickness (approximately nanomat thickness), as shown in Figure 64.

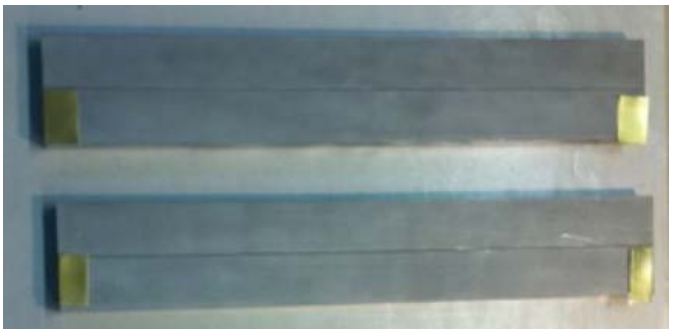

Figure 64 – Copper laminates placed in the adherends ends.

Teflon laminates are put at one end of the bonding surface in order to obtain a pre-crack and thus to try to have cohesive failure inside the nano-reinforced resin.

One adherend is placed inside a plastic container; resin is spread on it using a spatula and a needle is necessary to break eventually formed bubbles. After that, the other adherend is bonded with the first one; once formed the joint, the specimen is wrapped into a Teflon sheet and placed inside a homemade aluminium template, as shown in Figure 65 and Figure 66.

Figure 65 – Homemade aluminium template.

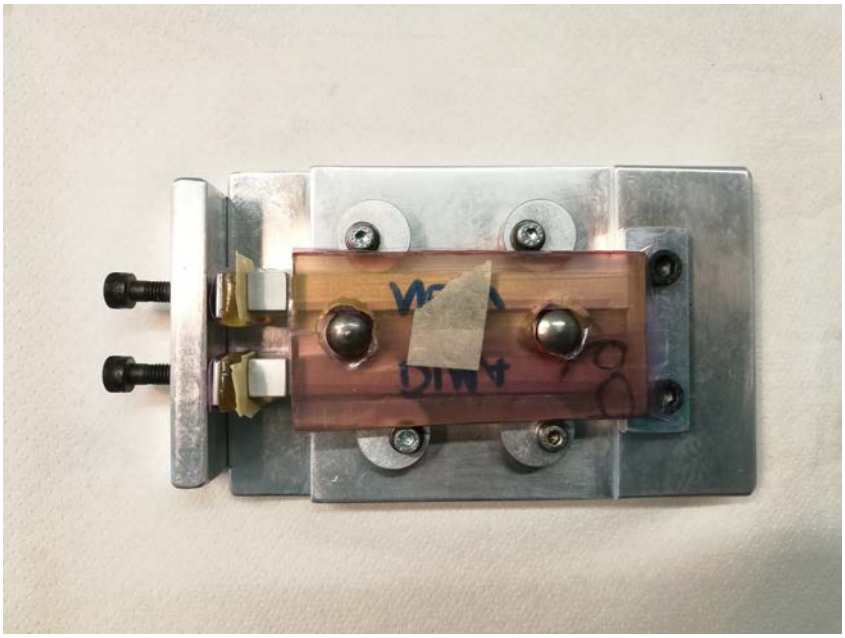

Figure 66 – Joints wrapped into Teflon sheets and put in the aluminium template.

The template has been developed in order to avoid the movement of the joints; at the same time, placing rubber spacers, is useful to avoid problems caused by thermal expansion. The piece of rubber put on the upper side of the joints allow the homogeneous distribution of the weight during curing.
It is particularly complex to join the two adherends in the virgin batches, because they tend to slip one on another; this doesn't happen with nano-reinforced ones because there is no excess of resin.

Nanofibers batches (N)

The nanofibers strip previously prepared is cut through its thickness with the help of paper tape and a lancet and a 350x12mm^2 band of Teflon is placed between the two patches of nanofibers as shown in Figure 68; paper tape is used to lock this configuration and avoid nanofibers stretching or deformation as demonstrated in Figure 69.

Figure 67 – Cut nanofibers mat.

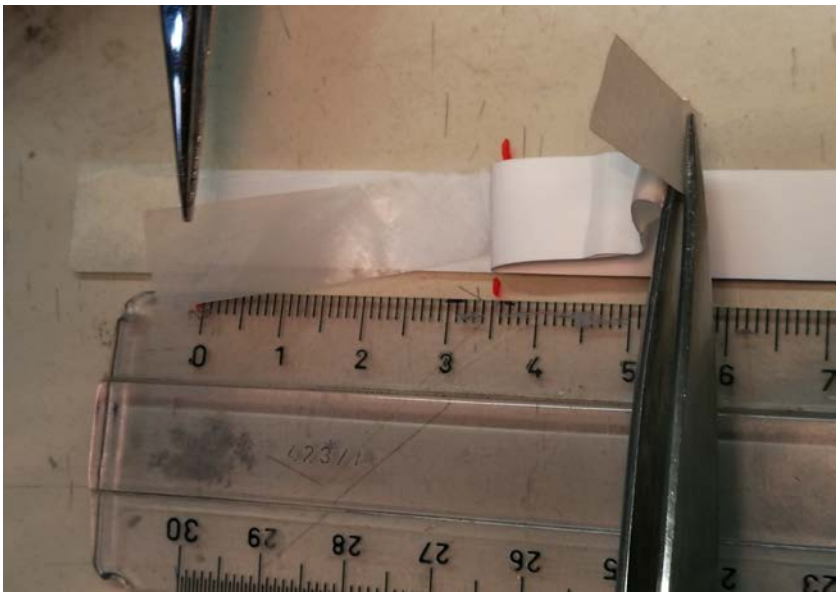

Figure 68 – Teflon strip placed inside nanofibers mat.

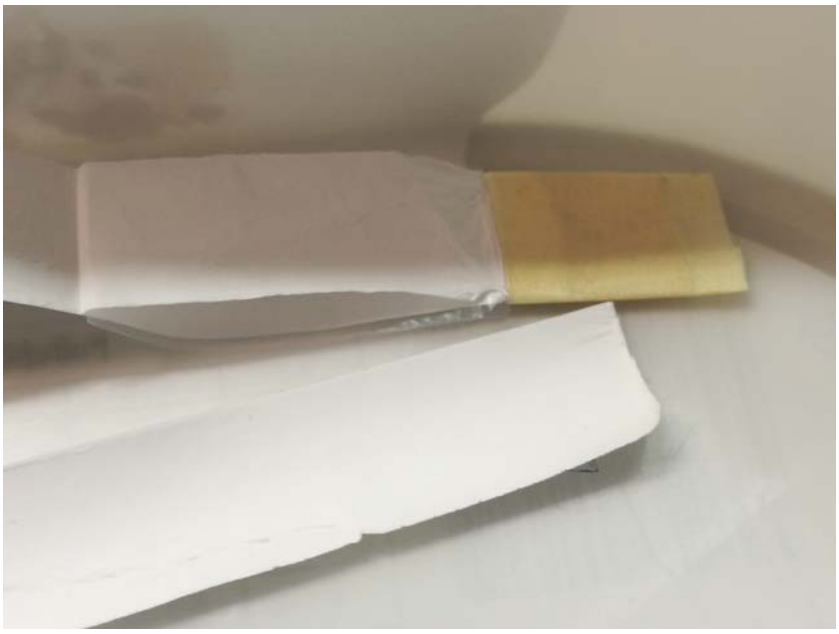

Figure 69 – Configuration with Teflon sheet placed inside the nanomat.

The strip is now placed into a plastic container and a small quantity of resin is poured on it and spread with a spatula, with the purpose of obtain an optimal impregnation.
Now, the wet nanomat and the quantity of resin is calibrated with two motorized, counter-rotating drums, showed in Figure 70; in this way is possible to obtain a sort of *nanofibers prepreg*.

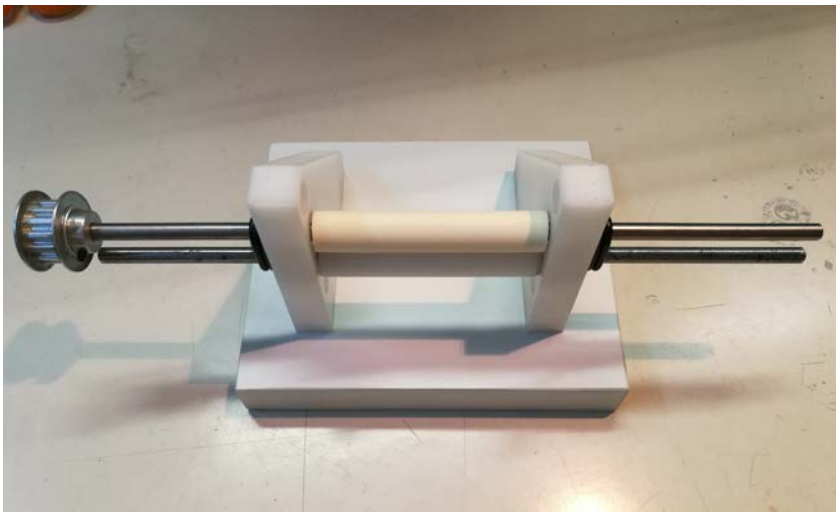

Figure 70 – Counter-rotating drums used to produce nanofibers prepreg.

At this point the strip is placed onto the surface of on adherend, bubbles are popped with a needle and the other adherend is bonded with the first one as shown in Figure 71.

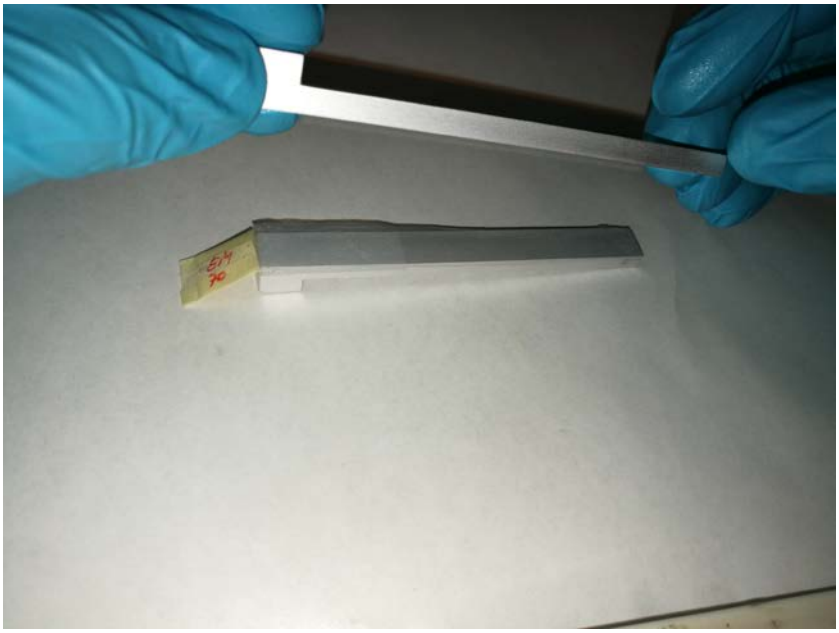

Figure 71 – Joining the two adherends.

Once the joint is made, the specimen is wrapped into a Teflon sheet and placed inside a homemade aluminium template, as shown in Figure 66.

5.4.1 Curing

Looking at the results obtained and described in Section 3.1.3, the following curing ramp has been selected:

1) T_{room} → 70°C (0.5°C/min)
2) 3h @70°C
3) Cooling inside the switched off oven

5.4.2 Thickness measures

The thickness of the nanomat is evaluated before and after integration in the joints.

Once the nanofibers mat is produced, its thickness is measured using a digital indicator, reported in Figure 72 with a 0.65 N preload, resolution of 1 μm, max error of 4 μm and repeatability of 2 μm.

Figure 72 – Digital indicator to measure thickness.

For what concerns thickness measures of cured nanomat, it is done using a scanning electron microscope (SEM); three different treatments were tried on the specimen section in order to better appreciate the presence of nanofibers all through the bonding section.

The three surface treatments are:

1) Rubbing with paper drenched with formic acid;
2) Cleaning with acetone;
3) Specimen left immersed in formic acid for 1 hour.

Results of these methods are reported in Section 3.3.
In the end, also the thickness of the cured specimen (adherend-adhesive-adherend) is measured using a digital callipers.

5.5 DCB tests

As it was described in section 1.8, DCB test is used to obtain the mode I fracture energy of adhesive bonds. Then, in addition to the displacement value acquired by the instrument, also the CMOD (which evaluates the resistance of a material to the propagation of a crack) is analysed by installing a clip-gage on the specimen.

6. REFERENCES

[1] *Adhesives Technology Handbook*, 2nd ed. Norwich, NY, USA: William Andrew Pub, 2008.

[2] S. Prolongo, M. Gude, and A. Ureña, *Nanoreinforced Adhesives*, no. February. 2010.

[3] E. M. Petrie, *Handbook Of Adhesive and Sealants*. McGraw - Hill Handbooks, 1993.

[4] A. J. Kinloch, *Adhesion and adhesives: Science and technology*. Chapman and Hall, 1988.

[5] Edward M. Petrie, *Handbook of Adhesives and Sealants*. 2013.

[6] *Chemistry and Technology of Epoxy Resins*. Sheffield, UK: Springer Science+Business Media Dordrecht Pub., 1993.

[7] T. M. Brugo, “Fracture toughening and self-healing of composite laminates by nanofibrous mats interleaving,” 2017.

[8] Nasikhudin, M. Diantoro, A. Kusumaatmaja, and K. Triyana, “Study on Photocatalytic Properties of TiO2 Nanoparticle in various pH condition,” in *Journal of Physics: Conference Series*, 2018.

[9] A. Dorigato and A. Pegoretti, “The role of alumina nanoparticles in epoxy adhesives,” *J. Nanoparticle Res.*, vol. 13, no. 6, pp. 2429–2441, 2011.

[10] Q. Meng *et al.*, “Toughening polymer adhesives using nanosized elastomeric particles,” *J. Mater. Res.*, vol. 29, no. 5, pp. 665–674, 2014.

[11] A. Buchman, H. Dodiuk-Kenig, A. Dotan, R. Tenne, and S. Kenig, “Toughening of epoxy adhesives by nanoparticles,” *J. Adhes. Sci. Technol.*, vol. 23, no. 5, pp. 753–768, 2009.

[12] “http://www.nanochemistry.science.” .

[13] H. Khoramishad, M. Ebrahimijamal, and M. Fasihi, “The effect of graphene oxide nano-platelets on fracture behavior of adhesively bonded joints,” *Fatigue Fract. Eng. Mater. Struct.*, vol. 40, no. 11, pp. 1905–1916, 2017.

[14] “https://worldofnanoscience.weebly.com/nanotube--carbon-fiber-overview.html.” .

[15] H. Khoramishad and D. Zarifpour, “Fracture response of adhesive joints reinforced with aligned multi-walled carbon nanotubes using an external electric field,” *Theor. Appl. Fract. Mech.*, vol. 98, no. October, pp. 220–229,

2018.

[16] P. K. Panda and S. Ramakrishna, “Electrospinning of alumina nanofibers using different precursors,” in *Journal of Materials Science*, 2007.

[17] S. Mohammadzadehmoghadam, Y. Dong, and I. Jeffery Davies, “Recent progress in electrospun nanofibers: Reinforcement effect and mechanical performance,” *J. Polym. Sci. Part B Polym. Phys.*, vol. 53, no. 17, pp. 1171–1212, 2015.

[18] G. Wang, D. Yu, A. D. Kelkar, and L. Zhang, “Electrospun nanofiber: Emerging reinforcing filler in polymer matrix composite materials,” *Prog. Polym. Sci.*, vol. 75, pp. 73–107, 2017.

[19] R. Palazzetti and A. Zucchelli, “Electrospun nanofibers as reinforcement for composite laminates materials – A review,” *Composite Structures*. 2017.

[20] Q. Chen, W. Wu, Y. Zhao, M. Xi, T. Xu, and H. Fong, “Nano-epoxy resins containing electrospun carbon nanofibers and the resulting hybrid multi-scale composites,” *Compos. Part B Eng.*, vol. 58, pp. 43–53, 2014.

[21] X. Gao, J. Lan, X. Jia, Q. Cai, and X. Yang, “Improving interfacial adhesion with epoxy matrix using hybridized carbon nanofibers containing calcium phosphate nanoparticles for bone repairing,” *Mater. Sci. Eng. C*, vol. 61, pp. 174–179, 2016.

[22] X. F. Wu *et al.*, “Electrospinning core-shell nanofibers for interfacial toughening and self-healing of carbon-fiber/epoxy composites,” *J. Appl. Polym. Sci.*, vol. 129, no. 3, pp. 1383–1393, 2013.

[23] F. Musiari *et al.*, “Experimental investigation on the enhancement of Mode I fracture toughness of adhesive bonded joints by electrospun nanofibers,” *J. Adhes.*, vol. 94, no. 11, pp. 974–990, 2018.

[24] D. M. T. M. Brugo, F. Musiari, A. Pirondi, A. Zucchelli, D. Cocchi, “Development and fracture toughness characterization of a nylon nanomat epoxy adhesive reinforcement,” *Proc. Inst. Mech. Eng. Part L J. Mater. Des. Appl.*, 2018.

[25] Z. Huang, Y. Zhang, M. Kotaki, and S. Ramakrishna, “A review on polymer nanofibers by electrospinning and their applications in nanocomposites,” vol. 63, pp. 2223–2253, 2003.

[26] T. Ondarcuhu *et al.*, “Drawing a single nanofibre over hundreds of microns,” 1998.

[27] K. Koenig, K. Beukenberg, F. Langensiepen, and G. Seide, “A new prototype

melt-electrospinning device for the production of biobased thermoplastic sub-microfibers and nanofibers," *Biomater. Res.*, vol. 23, no. 1, pp. 1–12, 2019.

[28] C. Díaz Muñiz, "Experimental investigation on the enhancement of mode i fracture toughness of adhesive bonded joints by electrospun nanofibers," Università di Bologna, 2018.

[29] J. V. Patil, S. S. Mali, A. S. Kamble, C. K. Hong, J. H. Kim, and P. S. Patil, "Electrospinning: A versatile technique for making of 1D growth of nanostructured nanofibers and its applications: An experimental approach," *Appl. Surf. Sci.*, vol. 423, pp. 641–674, 2017.

[30] C. He, W. Nie, and W. Feng, "Engineering of biomimetic nanofibrous matrices for drug delivery and tissue engineering," *J. Mater. Chem. B*, vol. 2, no. 45, pp. 7828–7848, 2014.

[31] T. J. Mitchison *et al.*, "Self-Assembly and Mineralization of Peptide-Amphiphile Nanofibers," vol. 649, 2001.

[32] J. Stanger, N. Tucker, and M. Staiger, "Electrospinning," vol. 16, no. 10, 2005.

[33] Geoffrey R. Mitchell, Ed., *Electrospinning - Principles, Practice and Possibilities*. 2015.

[34] H. Fong, I. Chun, and D. H. Reneker, "Beaded nanofibers formed during electrospinning," in *Polymer*, 1999.

[35] G. W. Critchlow and D. M. Brewis, "Review of surface pretreatments for aluminium alloys," vol. 16, no. 4, pp. 255–275, 1996.

[36] B. Chatterjee and R. W. Thomas, "Chemical Etching of Aluminium in Caustic Soda Solutions.," *Trans. Inst. Met. Finish.*, vol. 54, no. pt 1, pp. 17–24, 1976.

[37] R. F. Wegman, *Surface Preparation Techniques For Adhesive Bonding*. 1989.

[38] A. D. Juhl, "https://www.materialstoday.com/metal-finishing/features/anodizing-for-aerospace-101/." .

[39] C. H. P. M. F. Kanninen, "Advanced fracture mechanics," *Strain*, 1986.

[40] "Standard Test Method for Fracture Strength in Cleavage of Adhesives in Bonded Metal Joints," 2015.

[41] Q. Bai and Y. Bai, *Subsea Pipeline Design, Analysis, and Installation*. 2014.

[42] L. M. D. Cocchi, F. Musiari, T. M. Brugo, A. Pirondi, A. Zucchelli, F. Campanini, E. Leoni, "Characterization of aluminum alloy-epoxy bonded joints with nanofibers obtained by electrospinning," *J. Adhes.*, vol. 00, no. 00, pp. 1–18, 2019.

[43] S. G. Prolongo and A. Ureña, “Effect of surface pre-treatment on the adhesive strength of epoxy-aluminium joints,” *Int. J. Adhes. Adhes.*, vol. 29, no. 1, pp. 23–31, 2009.

[44] J. Barkhimer, M. Erich, and G. Nair, “Effect of Time Delay Between Etching and Adhesive Bonding (‘Outlife’ Time) on Lap-Shear Strength of Aluminum Alloys Using Environmentally-Friendly P2 Etch,” pp. 1–35, 2015.

[45] I. Olefjord, “Basic processes of surface preparation and,” vol. 3, no. October, pp. 860–874, 1987.

[46] F. Musiari *et al.*, “Feasibility study of adhesive bonding reinforcement by electrospun nanofibers,” *Procedia Struct. Integr.*, vol. 2, pp. 112–119, 2016.

[47] B. Federico, “On the influence of polymeric nanofibers in laminated,” Università di Bologna, 2012.

[48] E. Maccaferri, L. Mazzocchetti, T. Benelli, A. Zucchelli, and L. Giorgini, “Morphology, thermal, mechanical properties and ageing of nylon 6,6/graphene nanofibers as Nano2 materials,” *Compos. Part B Eng.*, vol. 166, no. October 2018, pp. 120–129, 2019.